Supporting Information

Contents

1. Experimental details

General Considerations. All reactions and manipulations described below were carried out under anhydrous and anaerobic conditions using standard Schlenk line techniques and Ar-filled glove box. Tetrahydrofuran (THF), toluene, hexanes, and diethyl ether (Et_2O) were degassed and dehydrated by MBraun solvent purification system; dry dichloromethane (DCM) were obtained through distillation over CaH_2 followed by freeze-pump-thaw cycle. THF-d_8 were purchased from CIL and were redistilled over sodium. Cyclooctatetraene (COT) were purchased from Strem and were redistilled under vacuum to remove the stabilizer BHT. Ultra-dry ErI_3, potassium, zirconocene dichloride (Cp_2ZrCl_2), 1-trimethylsilylpropyne, ^{n}BuLi (2.5 M in hexanes), PCl_3 (2.0 M in DCM) were commercially available and used as received. 3,4-dimethyl-2,5-bis(trimethylsilyl)-phospholyl potassium (KDsp) was prepared according to literature [1] with slight modifications. ErICOT(THF)$_x$ ($x \approx 2.5$, Anal. Calc.: C, 37.37%; H, 4.87%; found: C, 36.93%; H, 4.65%.) was prepared by the reaction of ErI_3 with K_2COT [2] in THF.

^{1}H NMR and ^{31}P NMR spectra were recorded on a Bruker-500 MHz NMR spectrometer. Organometallic samples for NMR spectroscopic measurements were prepared in the glovebox using J. Young valve NMR tubes (Wilmad 528-JY). Before ^{31}P NMR experiment, a sealed thin glass tube containing 85% H_3PO_4 was put into the NMR tube containing the THF-d_8 solution of sample as the external standard. Elemental analyses were performed on the Vario EL CUBE Elemental Analyzer.

Synthesis of (Dsp)Er(COT). 0.5786 g (1 mmol) of ErICOT(THF)$_{2.5}$ and 0.2946 g (1 mmol) of KDsp were dispersed in ca. 20 mL of toluene in a Schlenk tube followed by reflux under Ar overnight. After cooled to room temperature, the reaction solution was filtered to remove KI, and the filtrate was concentrated. Orange single crystals suitable for X-ray diffraction analysis were obtained by cooling the concentrated solution at –30 ºC. Yield: 0.2844 g, 53.97%. Analytically calculated for DspErCOT: C, 45.59%; H, 6.12%; found: C, 45.73%; H, 6.12%.

Following the similar procedure, single crystals of (Dsp)Y(COT), (Dsp)Tb(COT), (Dsp)Dy(COT), (Dsp)Tm(COT) can also be isolated with satisfactory yields.

2. Crystallographic Data

2.1 Data collection and refinement

The crystals were wrapped in mineral oil and then were frozen in 180 K. Data collections were performed at 180 K on a SuperNova diffractometer using graphite-monochromated Mo Kα radiation (λ = 0.71073 Å). Using Olex2 [3], the structure was solved with the Superflip structure solution program using Charge Flipping [4] and refined with the ShelXL refinement package using Least Squares minimization. Refinement was performed on F^2 anisotropically for all of the nonhydrogen atoms by the full-matrix least-squares method. The hydrogen atoms were placed at the calculated positions and were included in the structure calculation without further refinement of their parameters. COT rings in (Dsp)Tb(COT) and (Dsp)Dy(COT) were not disordered, while in (Dsp)Y(COT), (Dsp)Er(COT) and (Dsp)Tm(COT) were disordered at 180 K and were treated with 68.6% and 31.4% occupancy in (Dsp)Y(COT), 55.8% and 44.2% in (Dsp)Er(COT), and 60.7% and 39.3% in (Dsp)Tm(COT). Crystallographic data (excluding structure factors) have been deposited with the Cambridge Crystallographic Data Centre with supplementary publication numbers: 1835954 ~ 1835958. These data can be obtained free of charge from the Cambridge Crystallographic Data Centre via https://www.ccdc.cam.ac.uk/structures/.

2.2 Single crystal structure of (Dsp)RE(COT) (RE = Y, Tb, Dy, Er, Tm)

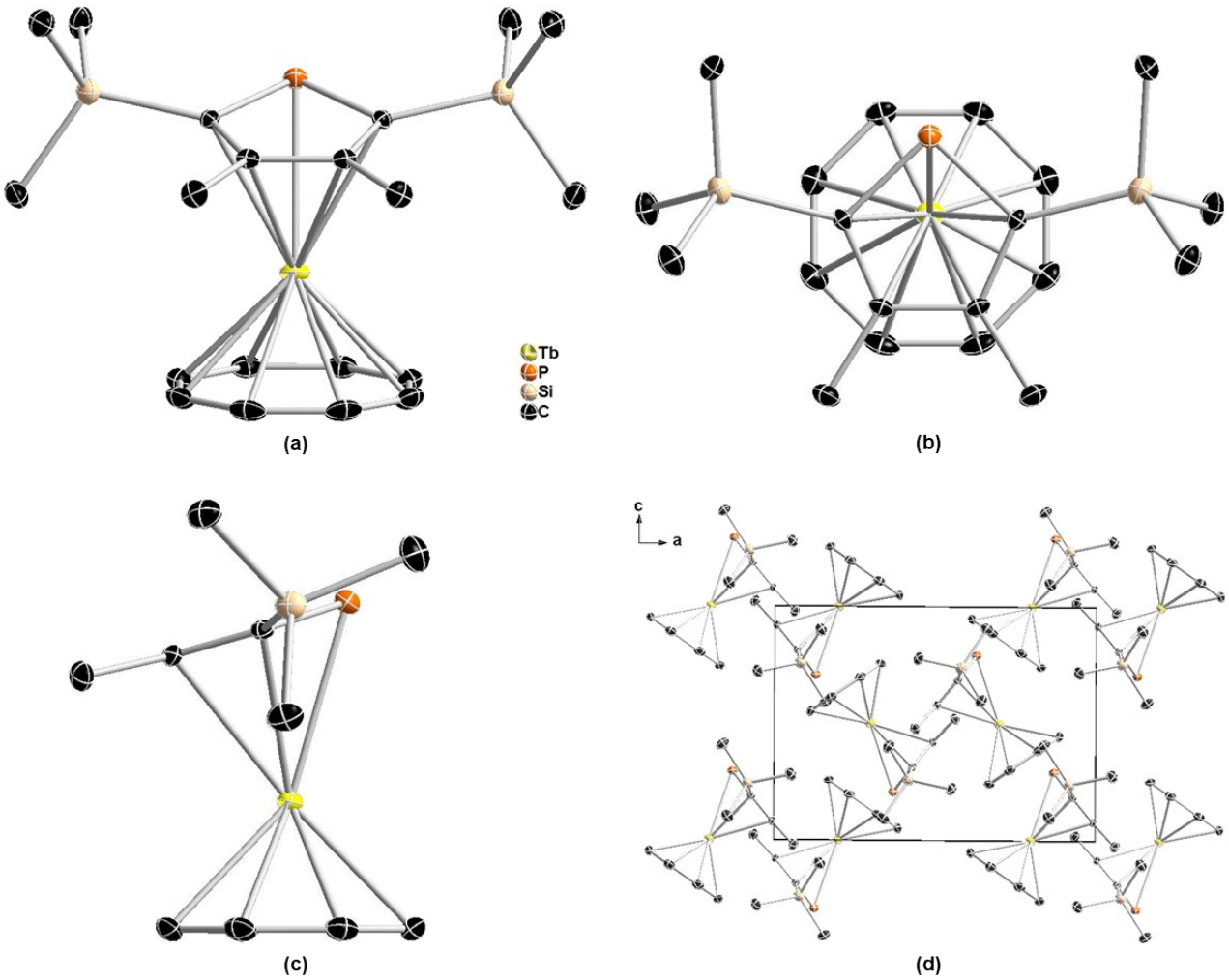

Figure S1. Front view **(a)**, top view **(b)**, side view **(c)** and packing diagram **(d)** of single crystal structure of **(Dsp)Tb(COT)** with yellow, orange, tan, and black ellipsoids (30% possibility) representing Tb, P, Si, and C, respectively. Hydrogen atoms have been omitted for clarity.

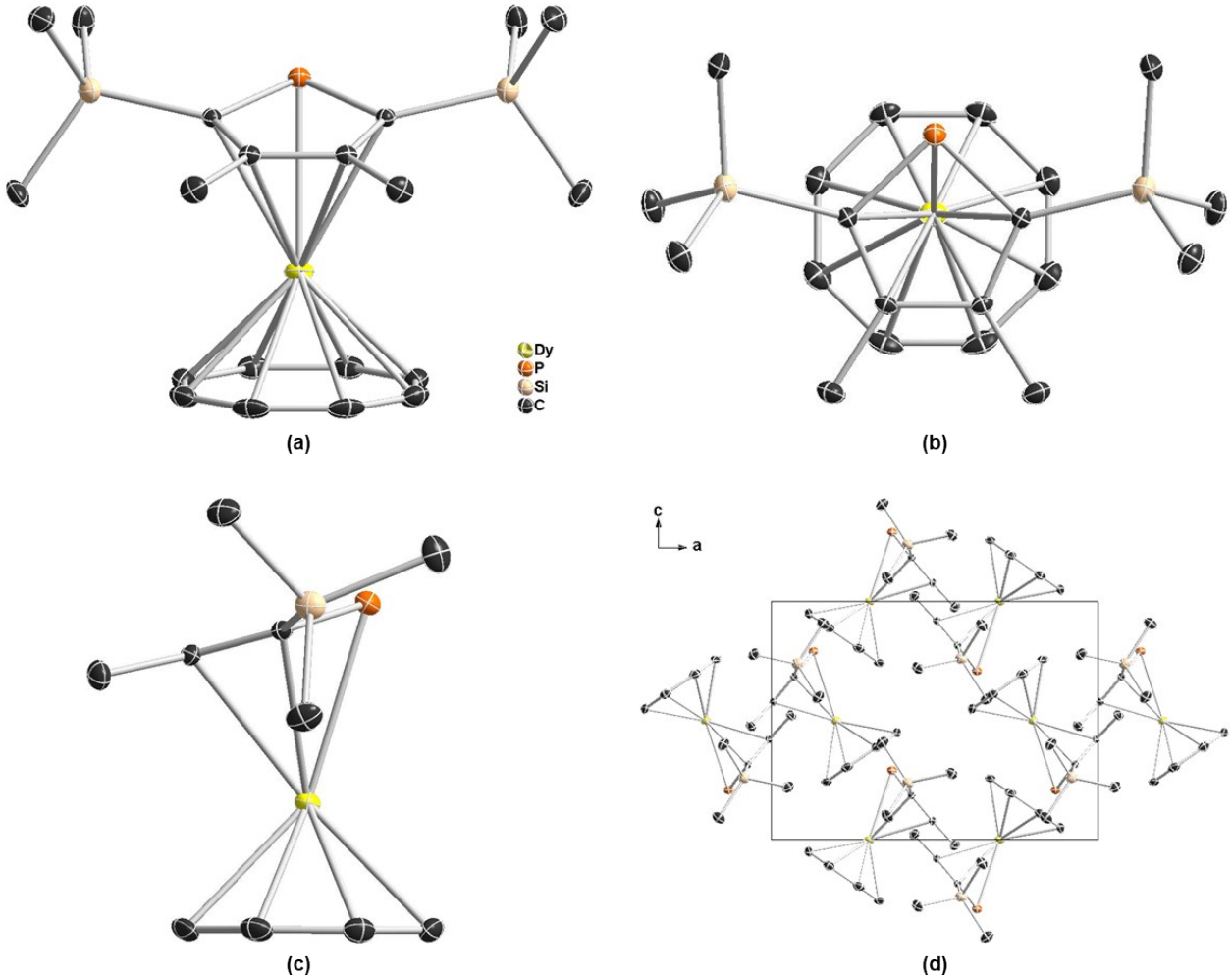

Figure S2. Front view **(a)**, top view **(b)**, side view **(c)** and packing diagram **(d)** of single crystal structure of **(Dsp)Dy(COT)** with yellow, orange, tan, and black ellipsoids (30% possibility) representing Dy, P, Si, and C, respectively. Hydrogen atoms have been omitted for clarity.

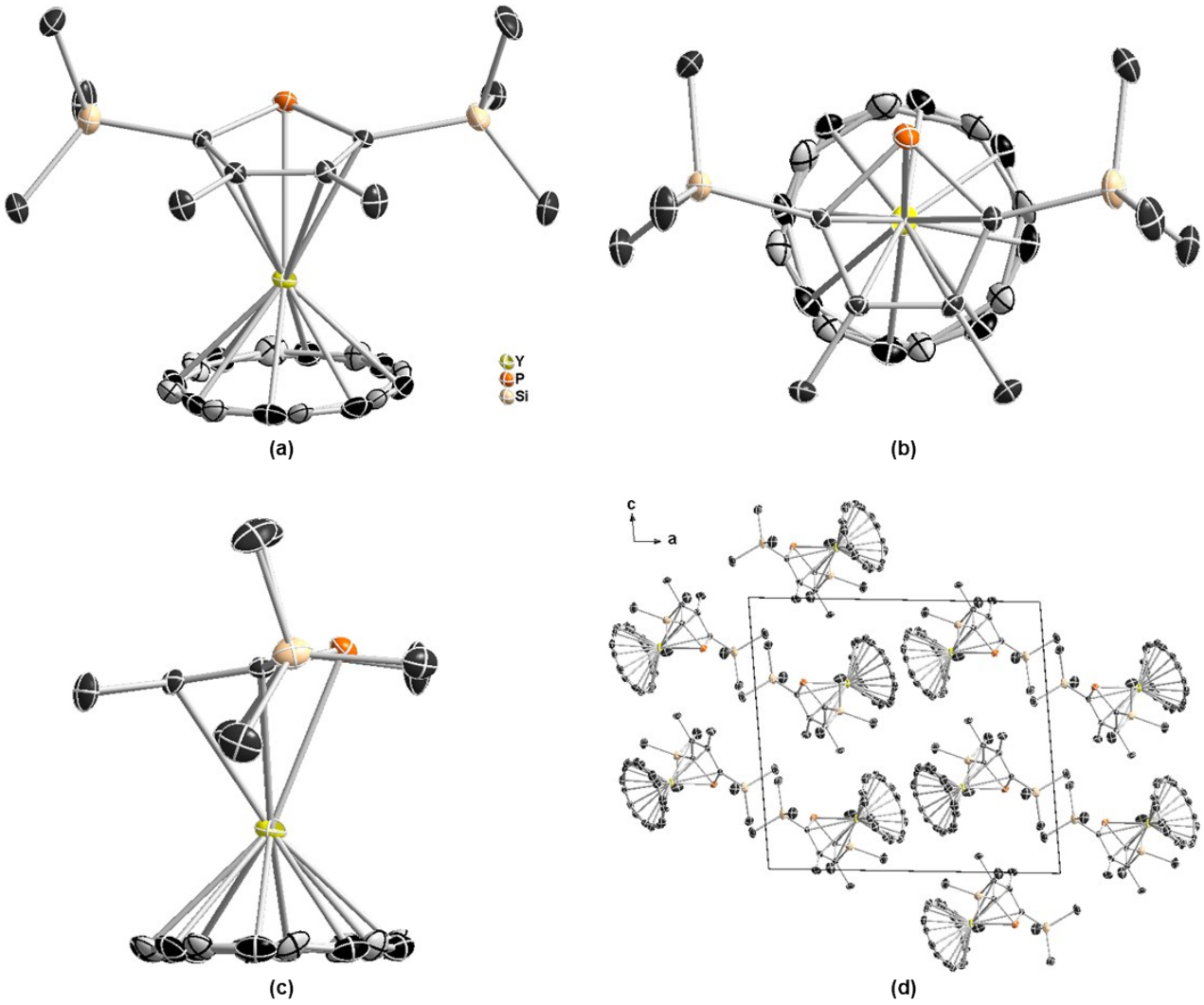

Figure S3. Front view **(a)**, top view **(b)**, side view **(c)** and packing diagram (**d**) of single crystal structure of **(Dsp)Y(COT)** with yellow, orange, tan, and black ellipsoids (30% possibility) representing Y, P, Si, and C, respectively, and the light grey ones are carbon atoms on another disorder fragment of COT. Hydrogen atoms have been omitted for clarity.

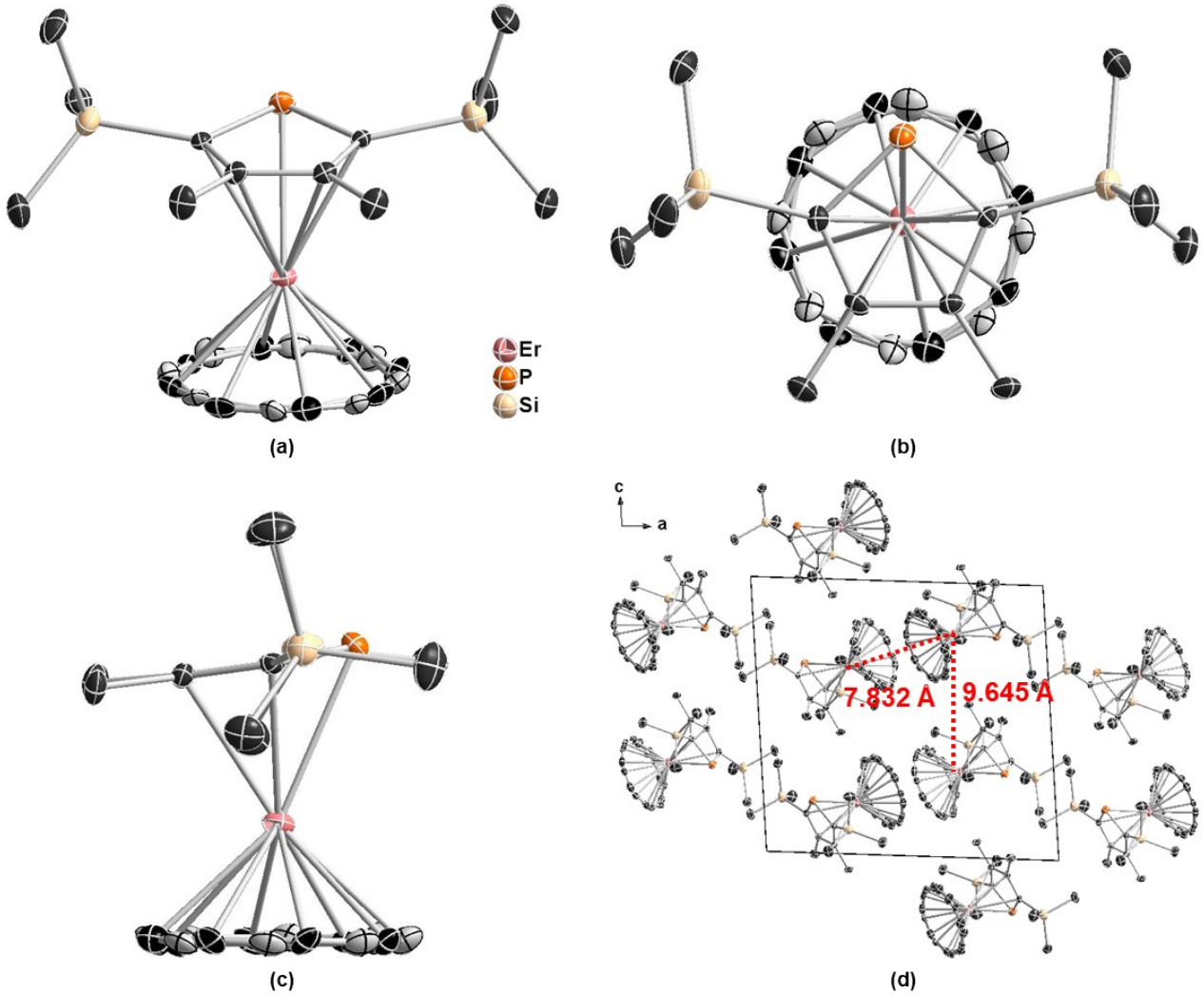

Figure S4. Front view **(a)**, top view **(b)**, side view **(c)** and packing diagram (**d**) of single crystal structure of **(Dsp)Er(COT)** with pink, orange, tan, and black ellipsoids (30% possibility) representing Er, P, Si, and C, respectively, and the light grey ones are carbon atoms on another disorder fragment of COT. Hydrogen atoms have been omitted for clarity.

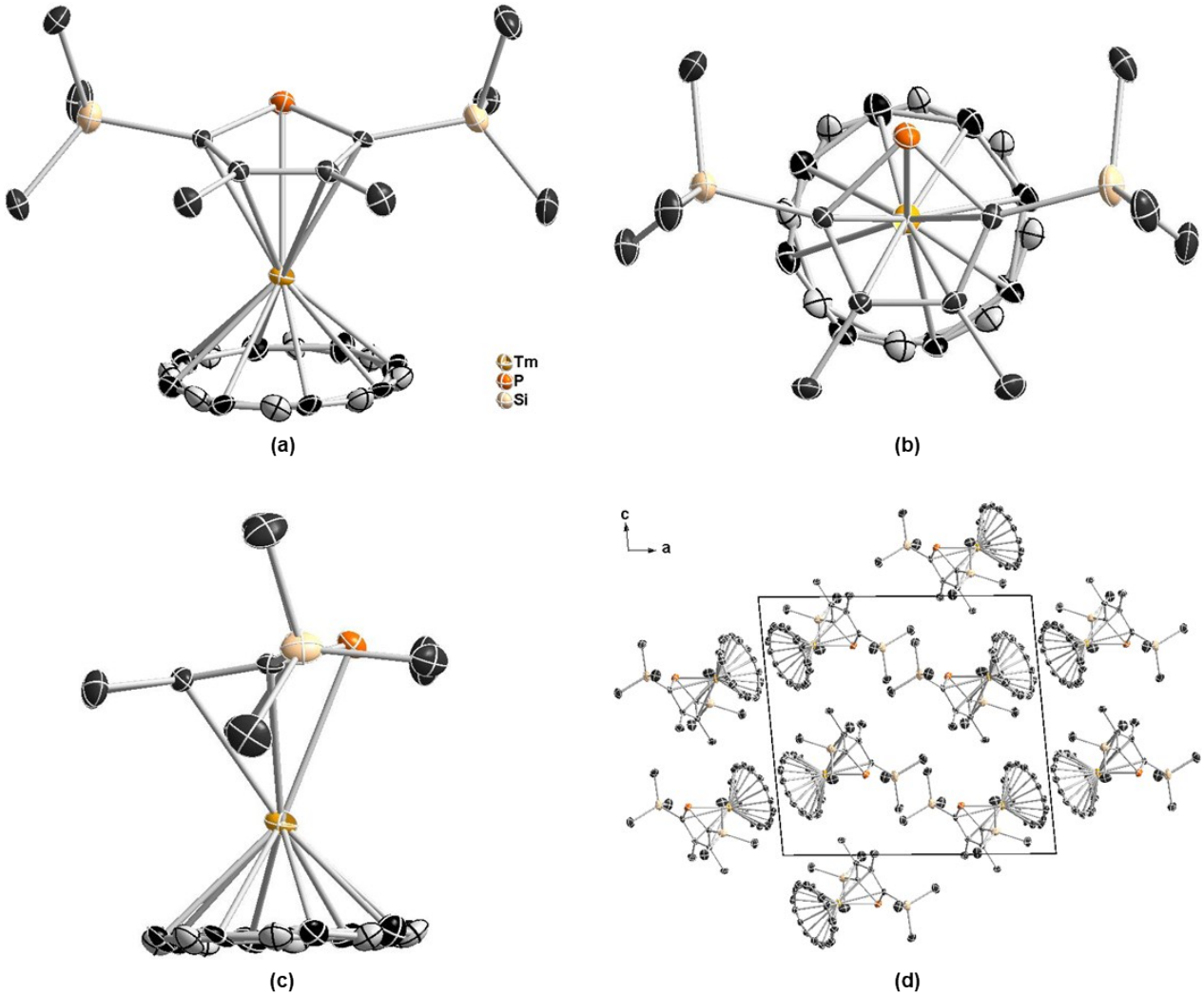

Figure S5. Front view **(a)**, top view **(b)**, side view **(c)** and packing diagram (**d**) of single crystal structure of **(Dsp)Tm(COT)** with dark yellow, orange, tan, and black ellipsoids (30% possibility) representing Tm, P, Si, and C, respectively, and the light grey ones are carbon atoms on another disorder fragment of COT. Hydrogen atoms have been omitted for clarity.

Table S1 Crystallographic data of (Dsp)RE(COT) (RE = Y, Tb, Dy, Er, Tm)

Formula	**$C_{20}H_{32}Si_2PTb$**	**$C_{20}H_{32}Si_2PDy$**	**$C_{20}H_{32}Si_2PY$**	**$C_{20}H_{32}Si_2PEr$**	**$C_{20}H_{32}Si_2PTm$**
Formula Weight	518.52	522.10	448.51	526.86	528.53
T, K	180	180	180	180	180
λ, Å	0.710	0.710	0.710	0.710	0.710
Crystal System	Orthorhombic	Orthorhombic	Monoclinic	Monoclinic	Monoclinic
Space Group	*Pnma*	*Pnma*	$P2_1/c$	$P2_1/c$	$P2_1/c$
a, Å	12.8319(7)	12.8248(7)	15.2388(7)	15.1266(6)	15.0719(8)
b, Å	18.8787(12)	18.9114(12)	10.8568(5)	10.8150(4)	10.8053(6)
c, Å	9.3269(5)	9.3047(4)	14.2170(8)	14.2560(8)	14.3183(9)
β, degree	90	90	95.180(4)	95.164(4)	95.125(5)
Z	4	4	4	4	4
V, Å^3	2259.4(2)	2256.7(2)	2342.5(2)	2322.73(19)	2322.5(2)
D_c, g cm^{-3}	1.524	1.537	1.272	1.507	1.512
F(000)	1040.0	1044.0	936.0	1052.0	1056.0
μ, mm^{-1}	3.307	3.488	2.660	3.785	3.992
R_{int}	0.0501	0.0548	0.0632	0.0401	0.0512
R_1(reflections)	0.0301(2197)	0.0324(2126)	0.0395(4926)	0.0356(4537)	0.0400(4208)
wR_2(reflections)	0.0587(3273)	0.0612(3233)	0.0730(6315)	0.0691(6138)	0.0723(6133)
S	1.082	1.076	1.018	1.091	1.045

Table S2 Selected bond lengths of (Dsp)RE(COT) (RE = Y, Tb, Dy, Er, Tm)

Bonds/Å	$C_{20}H_{32}Si_2PTb$	$C_{20}H_{32}Si_2PDy$	$C_{20}H_{32}Si_2PY$	$C_{20}H_{32}Si_2PEr$	$C_{20}H_{32}Si_2PTm$
RE-P1	2.874	2.858	2.826	2.793	2.782
RE-C1(C1B) (COT)	2.547	2.533	2.490 (2.549)	2.489 (2.516)	2.500 (2.426)
RE-C2(C2B) (COT)	2.543	2.535	2.480 (2.528)	2.491 (2.482)	2.514 (2.443)
RE-C3(C3B) (COT)	2.542	2.525	2.464 (2.533)	2.487 (2.472)	2.491 (2.446)
RE-C4(C4B) (COT)	2.533	2.519	2.490 (2.520)	2.510 (2.480)	2.495 (2.465)
RE-C5(C5B) (COT)	2.533	2.519	2.551 (2.523)	2.505 (2.529)	2.478 (2.522)
RE-C6(C6B) (COT)	2.542	2.525	2.559 (2.527)	2.471 (2.494)	2.462 (2.509)
RE-C7(C7B) (COT)	2.543	2.535	2.497 (2.534)	2.483 (2.499)	2.468 (2.450)
RE-C8(C8B) (COT)	2.547	2.533	2.480 (2.542)	2.497 (2.489)	2.501 (2.453)
RE-Centroid (COT)	1.758	1.742	1.724 (1.705)	1.698 (1.689)	1.668 (1.652)
C-C (COT)	1.395 ~ 1.416	1.397 ~ 1.406	1.395 ~ 1.403 (1.403 ~ 1.412)	1.400 ~ 1.410 (1.395 ~ 1.411)	1.397 ~ 1.414 (1.395 ~ 1.411)
RE-C9 (Dsp)	2.726	2.706	2.675	2.635	2.633
RE-C10 (Dsp)	2.695	2.679	2.671	2.638	2.628
RE-C11 (Dsp)	2.695	2.679	2.663	2.645	2.624
RE-C12 (Dsp)	2.726	2.706	2.671	2.642	2.632
RE-Centroid (Dsp)	2.403	2.383	2.354	2.321	2.302
C (adjacent)-P1 (Dsp)	1.775	1.776	1.771, 1.779	1.772, 1.769	1.776, 1.778
C-C (Dsp)	1.416 ~ 1.420	1.414 ~ 1.416	1.412 ~ 1.422	1.412 ~ 1.418	1.408 ~ 1.419
Shortest Ln - - - Ln	7.9352(5)	7.9282(5)	7.8758(5)	7.8315(4)	7.8097(5)

Table S3 Selected angles of (Dsp)RE(COT) (RE = Y, Tb, Dy, Er, Tm)

Angles /°	$C_{20}H_{32}Si_2PTb$	$C_{20}H_{32}Si_2PDy$	$C_{20}H_{32}Si_2PY$	$C_{20}H_{32}Si_2PEr$	$C_{20}H_{32}Si_2PTm$
C9-P1-C12	91.80	91.73	91.80	91.70	92.04
P1-C9-C10	110.57	110.45	110.46	110.84	109.94
C9-C10-C11	113.50	113.64	113.61	112.90	113.61
C10-C11-C12	113.50	113.64	113.30	113.93	114.06
P1-C12-C11	110.57	110.45	110.67	110.42	110.17
P1-C9, 10, 11, 12	1.70	1.95	2.22	2.49	3.01
Centroid (Dsp)-RE-Centroid (COT)	164.5	165.2	170.4 (170.2)	170.8 (170.8)	171.1 (169.4)

3. Magnetic properties

Samples were closely wrapped by two layers of para-films followed by plugged into a capsule in glovebox, and then fixed in a straw. This straw was placed in a Schlenk tube before being transferred out of glovebox. Direct current (DC) susceptibility and alternative current (AC) magnetic susceptibility with frequencies ranging from 1 to 997 Hz were performed on a Quantum Design MPMS2 XL-5 SQUID magnetometer on polycrystalline samples. AC susceptibility measurement with frequencies ranging from 100 to 10000 Hz was performed on a Quantum Design PPMS on polycrystalline samples. Magnetic hysteresis measurements were carried out on a Quantum Design MPMS3 SQUID magnetometer. All DC magnetic susceptibilities were corrected for diamagnetic contribution from the sample holder, para-films, capsules and diamagnetic contributions from the molecule using Pascal's constants [4].

3.1 Magnetic properties of DspErCOT

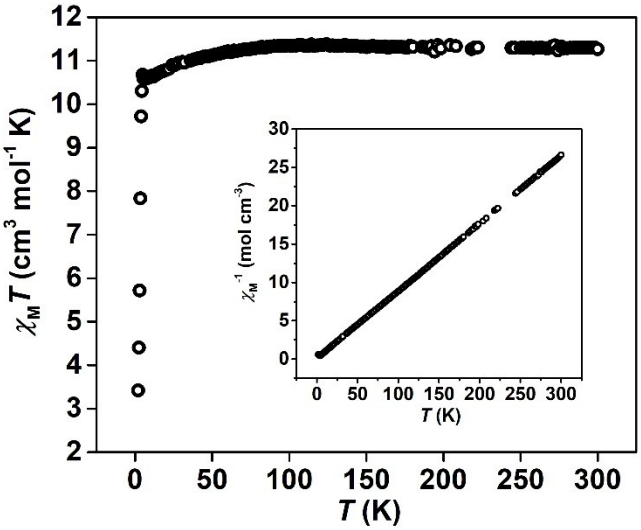

Figure S6. Temperature dependence of the static molar magnetic susceptibility times temperature ($\chi_M T$; inset: χ_M^{-1}) for **(Dsp)Er(COT)** under an applied static field of 1000 Oe over the temperature range from 2 to 300 K.

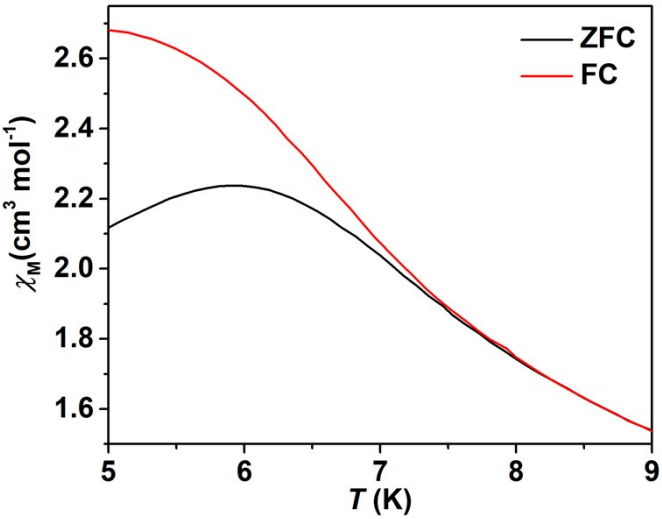

Figure S7. Plot of zero-field cooled (ZFC, black circles) and field-cooled (FC, red circles, H_{DC} = 1000 Oe) magnetic susceptibility of **(Dsp)Er(COT)** versus temperature.

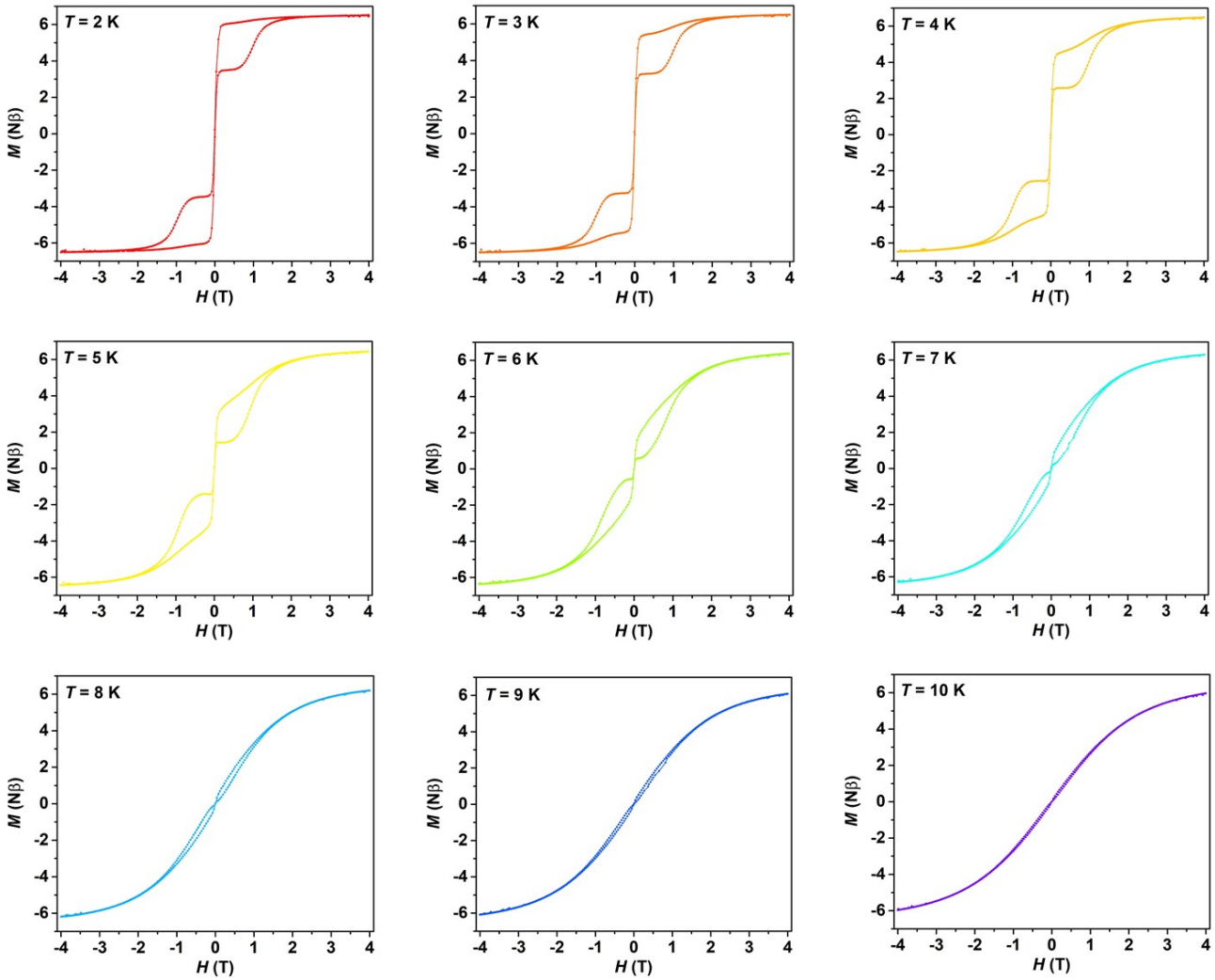

Figure S8. Magnetic hysteresis loops for **(Dsp)Er(COT)** with a field-sweeping rate of 200 Oe/s at 2, 3, 4, 5, 6, 7, 8, 9, 10 K, respectively.

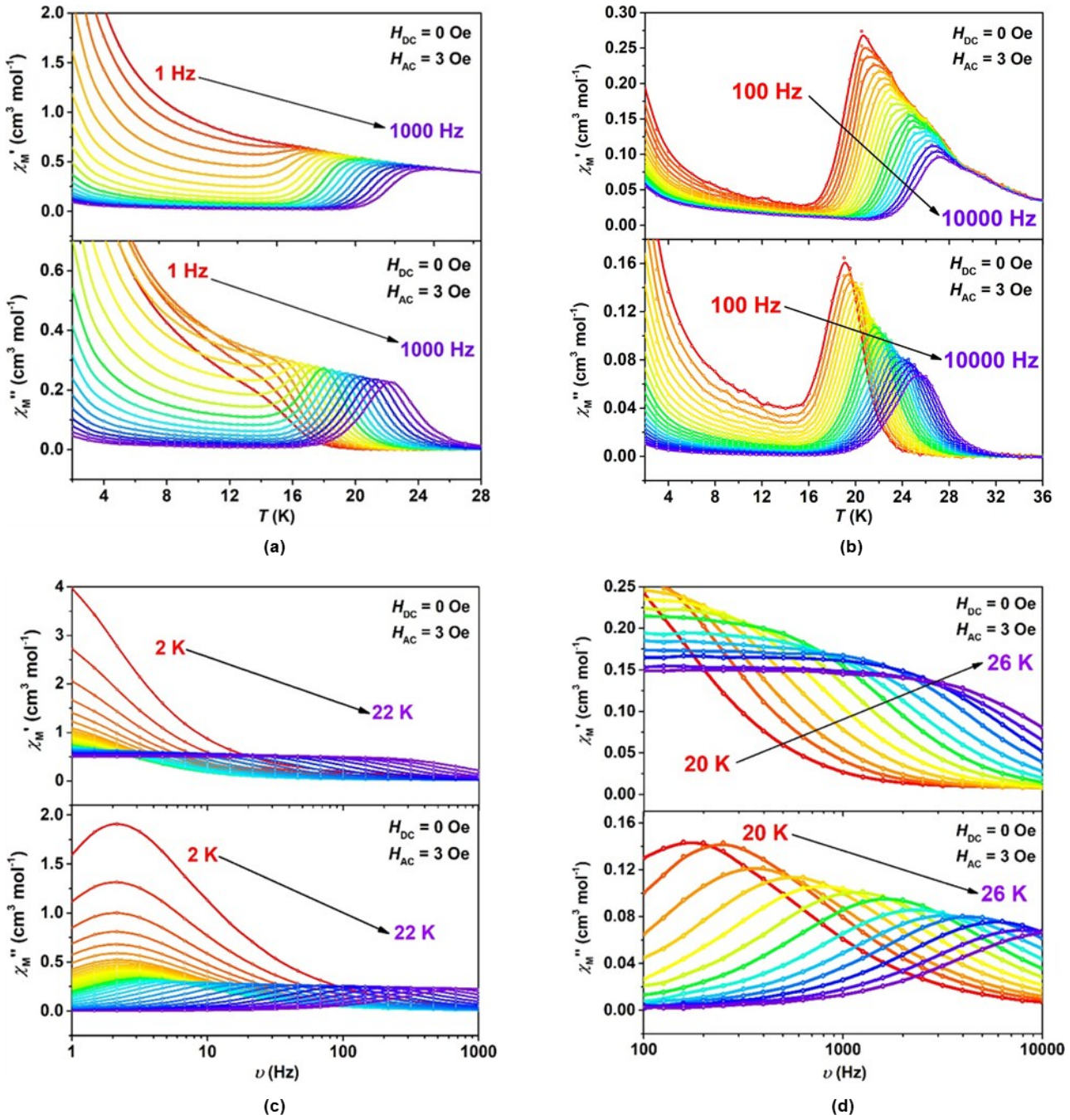

Figure S9. Temperature-dependence **(a, b)** and frequency-dependence **(c, d)** of in-phase (χ_M', upper) and out-of-phase (χ_M'', lower) molar AC susceptibility for **(Dsp)Er(COT)** under zero applied DC magnetic field. **(a, c)** are data derived from MPMS, and **(b, d)** are data derived from PPMS.

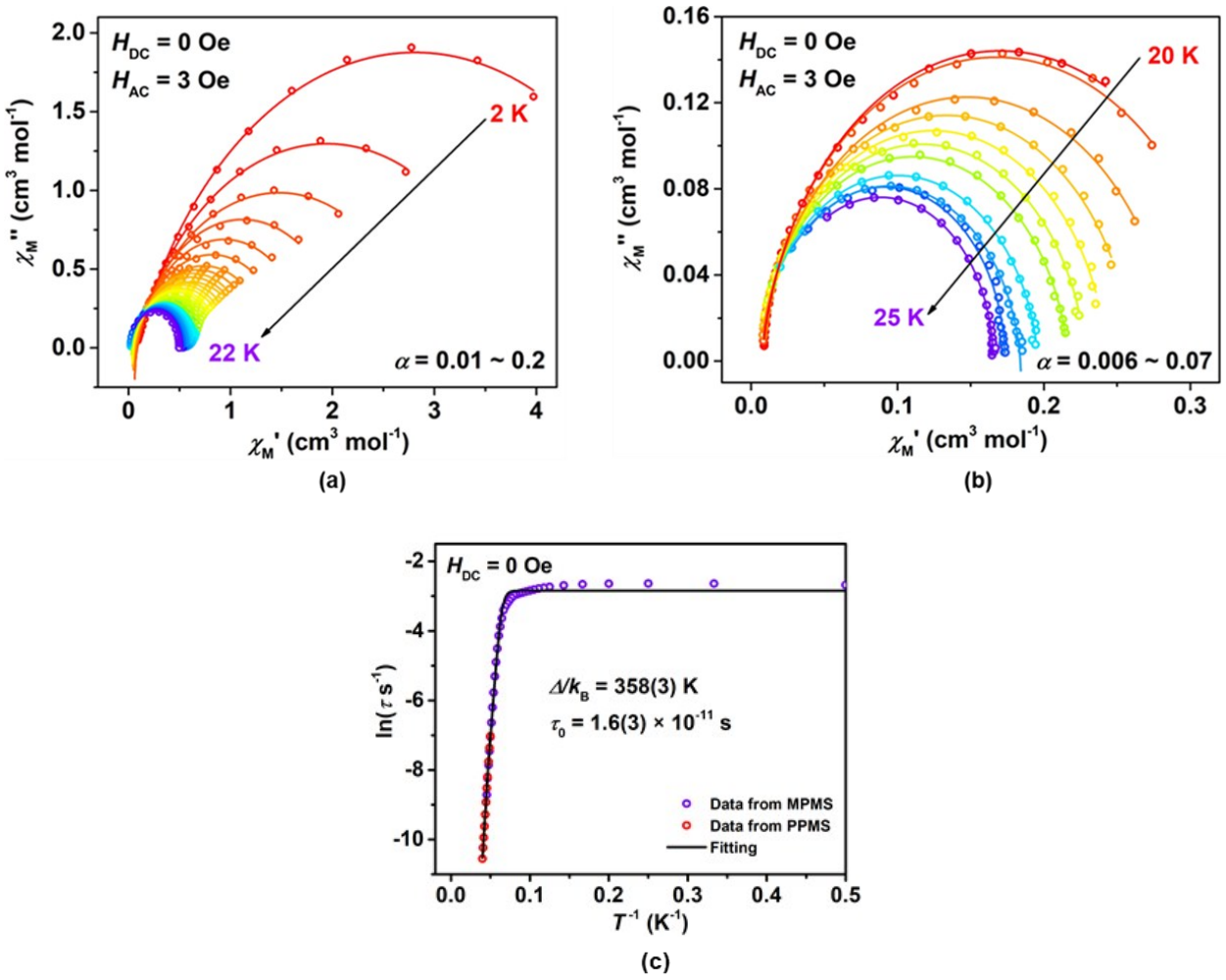

Figure S10. (a) and **(b)**: Argand plots of χ_M'' *vs* χ_M' of **(Dsp)Er(COT)** under zero applied DC magnetic field (**(a)** data derived from MPMS, **(b)** data derived from MPMS). **(c)** Plot of natural log of relaxation time versus inverse temperature. The red and purple circles represent the data from PPMS and MPMS, respectively. The black solid line represents the best fitting using a combination of Orbach and QTM process. The fitting gives energy barrier Δ/k_B = 358(3) K and τ_0 = 1.6(3) × 10^{-11} s.

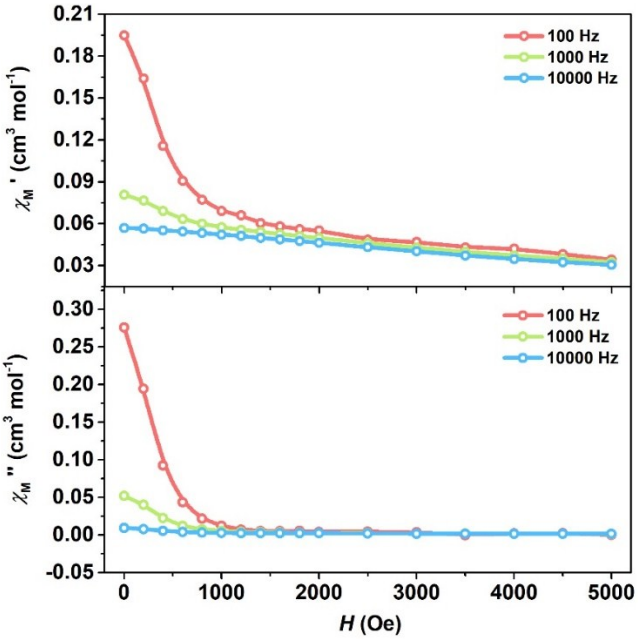

Figure S11. Plot of in-phase (χ_M', upper) and out-of-phase (χ_M'', lower) molar AC susceptibility for **(Dsp)Er(COT)** *vs* field under AC magnetic field with oscillated frequency of 100, 1000, 10000 Hz, respectively.

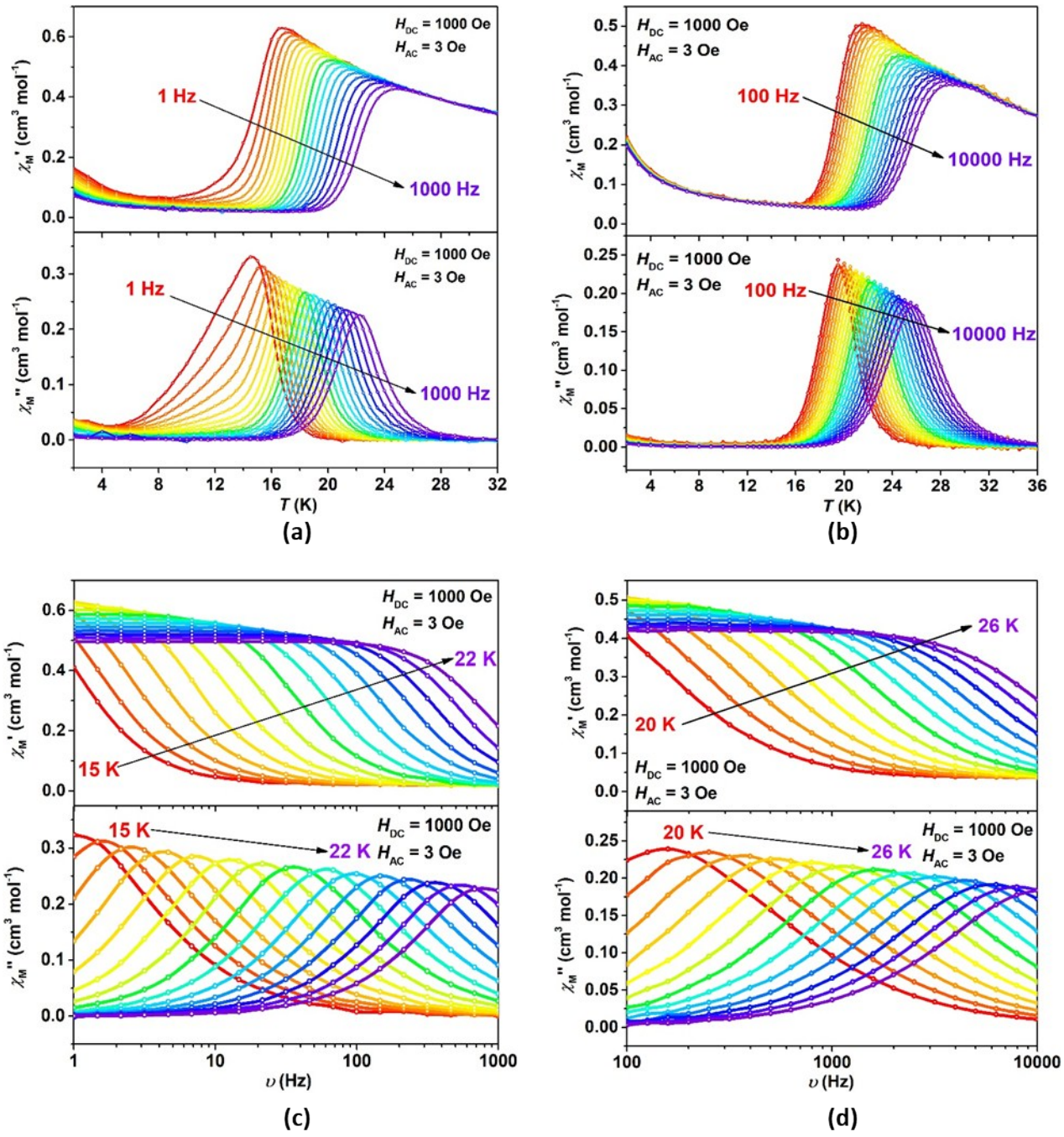

Figure S12. Temperature-dependence **(a, b)** and frequency-dependence **(c, d)** of in-phase (χ_M', upper) and out-of-phase (χ_M'', lower) molar AC susceptibility for **(Dsp)Er(COT)** under an applied DC magnetic field of 1000 Oe. **(a, c)** are data derived from MPMS, and **(b, d)** are data derived from PPMS.

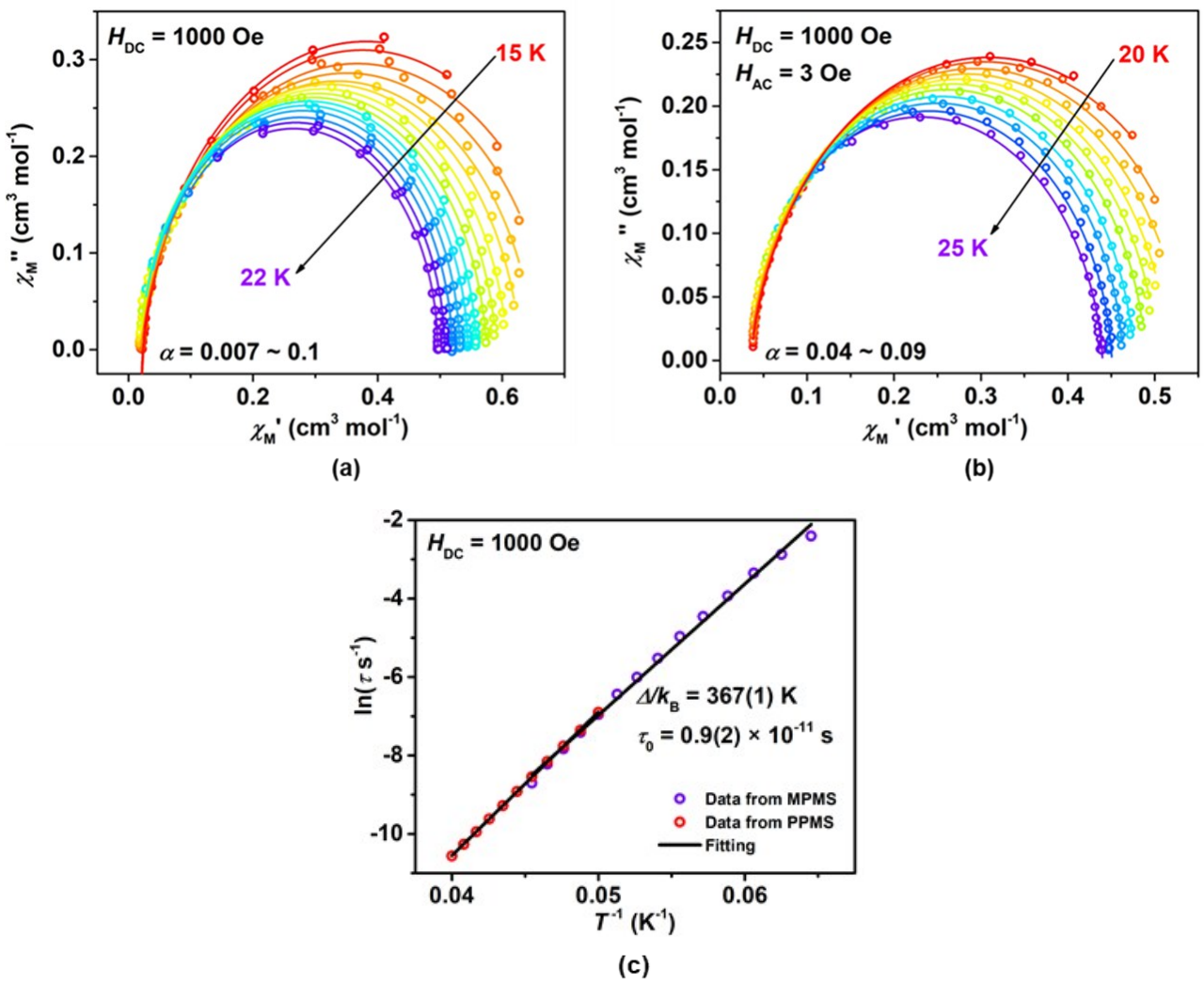

Figure S13. (a) and **(b)**: Argand plots of χ_M'' *vs* χ_M' of **(Dsp)Er(COT)** under an applied DC magnetic field of 1000 Oe (**(a)** data derived from MPMS, **(b)** data derived from MPMS). **(c)** Plot of natural log of relaxation time versus inverse temperature. The red and purple circles represent the data from PPMS and MPMS, respectively. The black solid line represents the best fitting using pure Orbach process. The fitting gives energy barrier Δ/k_B = 367(1) K and τ_0 = 0.9(2) × 10^{-11} s.

3.2. Magnetic properties of (Dsp)Dy(COT)

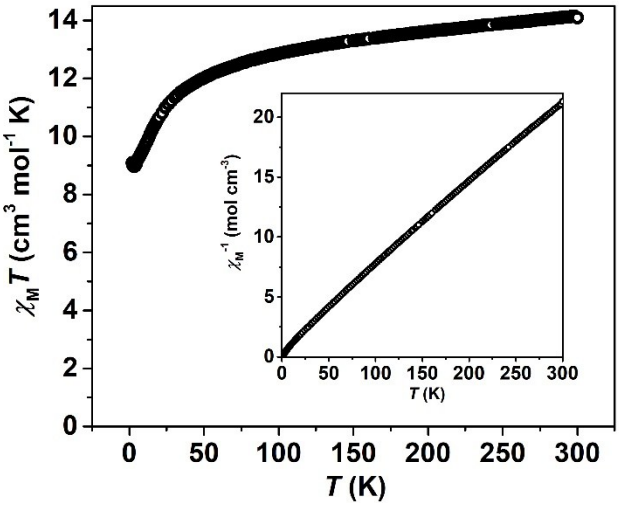

Figure S14. Temperature dependence of the static molar magnetic susceptibility times temperature ($\chi_M T$; inset, χ_M^{-1}) for **(Dsp)Dy(COT)** under an applied static field of 1000 Oe over the temperature range from 2 to 300 K.

The value of $\chi_M T$ for (Dsp)Dy(COT) at T = 300 K is 14.09 cm^3 mol^{-1} K, almost equals to that of a free Dy(III) ion (14.17 cm^3 mol^{-1} K).

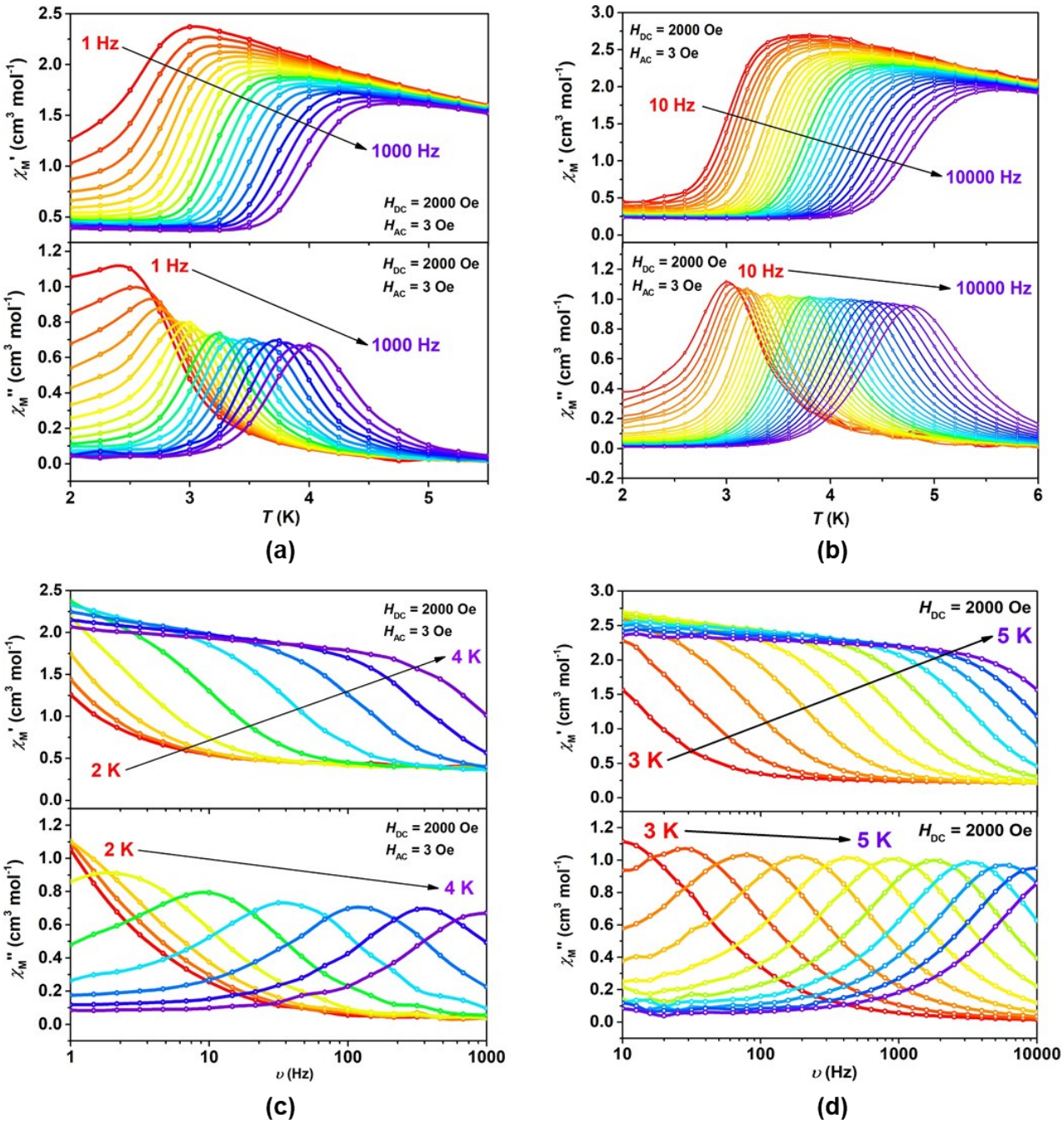

Figure S15. Temperature-dependence **(a, b)** and frequency-dependence **(c, d)** of in-phase (χ_M', upper) and out-of-phase (χ_M'', lower) molar AC susceptibility for **(Dsp)Dy(COT)** under an applied DC magnetic field of 1000 Oe. **(a, c)** are data derived from MPMS, and **(b, d)** are data derived from PPMS.

(Dsp)Dy(COT) doesn't show slow magnetic relaxation under zero applied DC field, that is, no frequency-dependence. So we don't show the data. The energy barrier under 2000 Oe DC field could be fitted using the combination of Orbach and Raman process, and returns 57 K (**Fig. S15**).

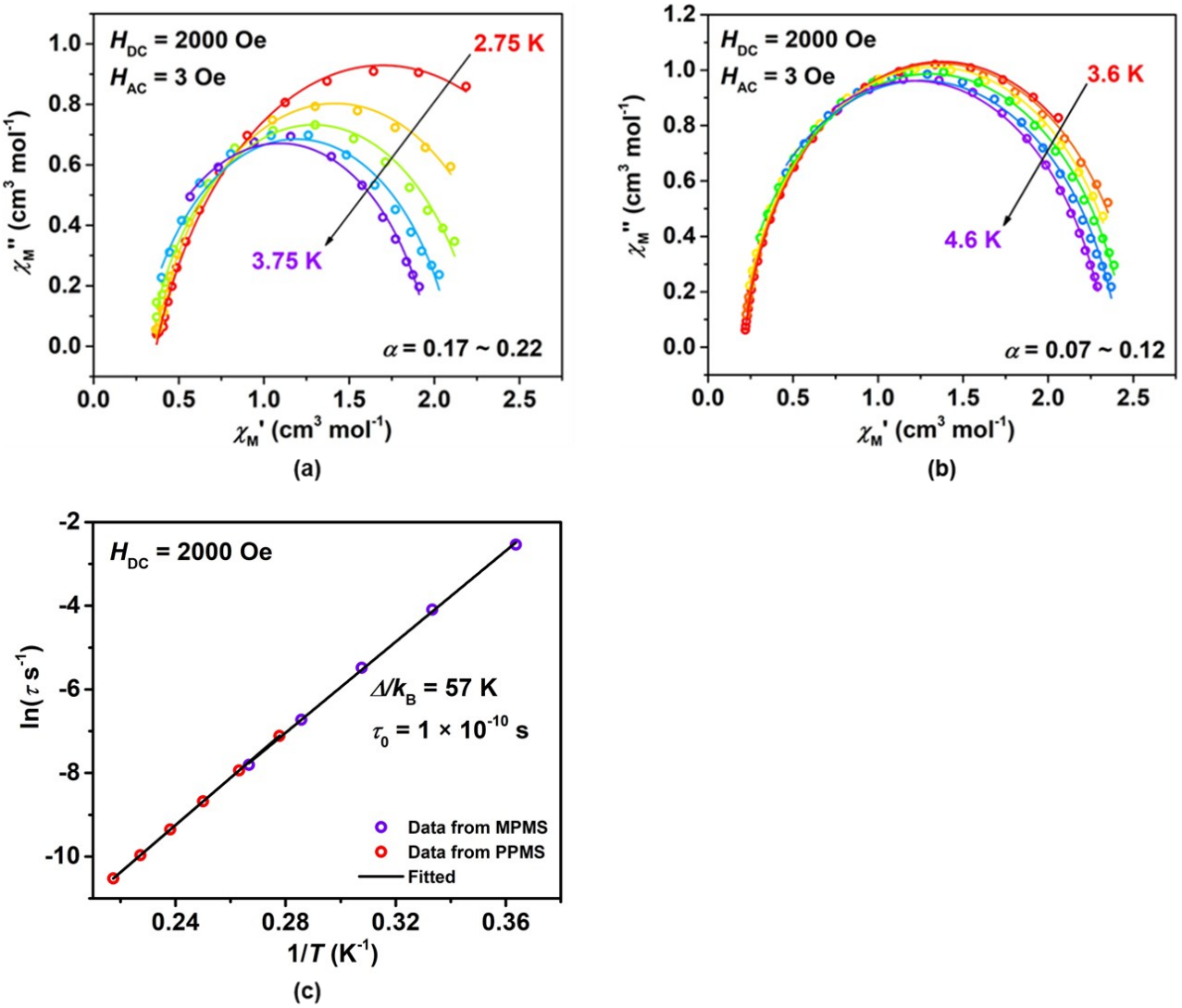

Figure S16. (a) and **(b)**: Argand plots of χ_M'' *vs* χ_M' of **(Dsp)Dy(COT)** under an applied DC magnetic field of 2000 Oe (**(a)** data derived from MPMS, **(b)** data derived from MPMS). **(c)** Plot of natural log of relaxation time versus inverse temperature. The red and purple circles represent the data from PPMS and MPMS, respectively. The black solid line represents the best fitting using pure Orbach process. The fitting gives energy barrier Δ/k_B = 57 K and $\tau_0 = 1 \times 10^{-11}$ s.

3.3. Magnetic properties of (Dsp)Tm(COT)

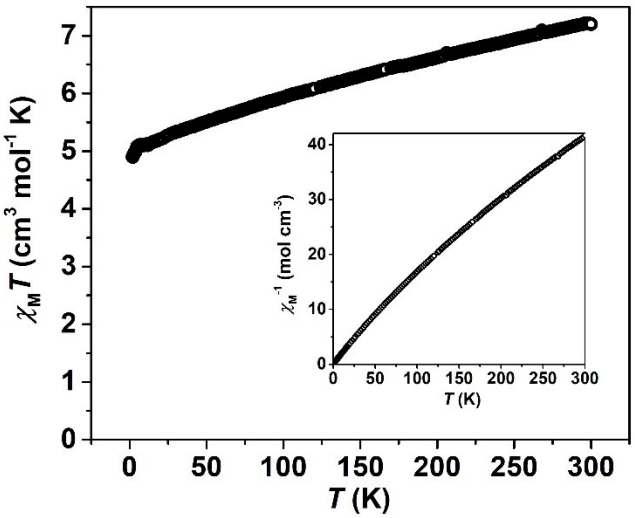

Figure S17. Temperature dependence of the static molar magnetic susceptibility times temperature ($\chi_M T$; inset, χ_M^{-1}) for **(Dsp)Tm(COT)** under an applied static field of 1000 Oe over the temperature range from 2 to 300 K.

The value of $\chi_M T$ for (Dsp)Tm(COT) at T = 300 K is 7.20 cm^3 mol^{-1} K, almost equals to that of a free Tm(III) ion (7.15 cm^3 mol^{-1} K).

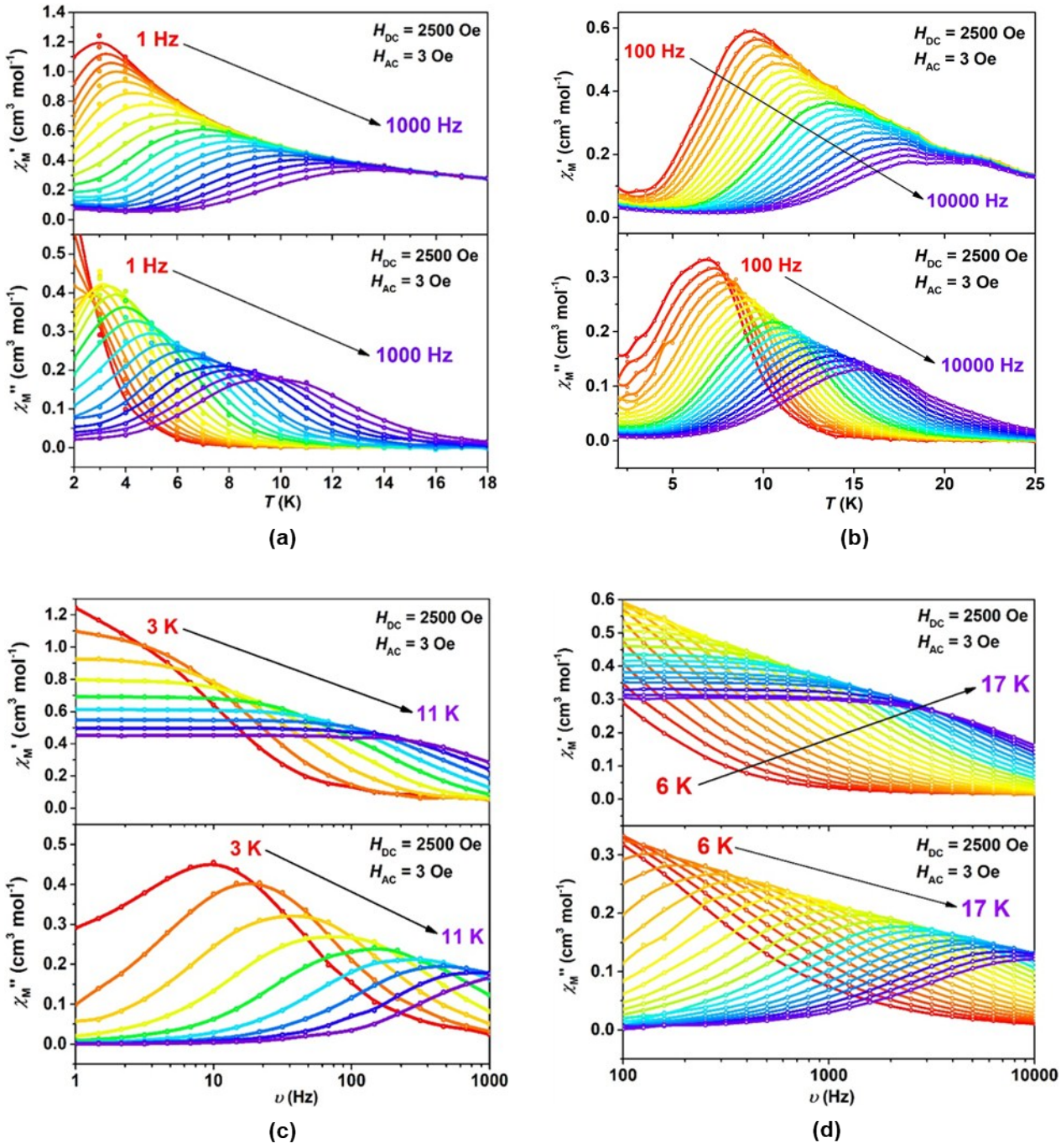

Figure S18. Temperature-dependence **(a, b)** and frequency-dependence **(c, d)** of in-phase (χ_M', upper) and out-of-phase (χ_M'', lower) molar AC susceptibility for **(Dsp)Tm(COT)** under an applied DC magnetic field of 2500 Oe. **(a, c)** are data derived from MPMS, and **(b, d)** are data derived from PPMS.

(Dsp)Tm(COT) doesn't show slow magnetic relaxation under zero applied DC field, that is, no frequency-dependence. So we don't show the data. The energy barrier under 2500 Oe DC field could be fitted using the combination of Orbach and Raman process, and returns 109 K (**Fig. S19**).

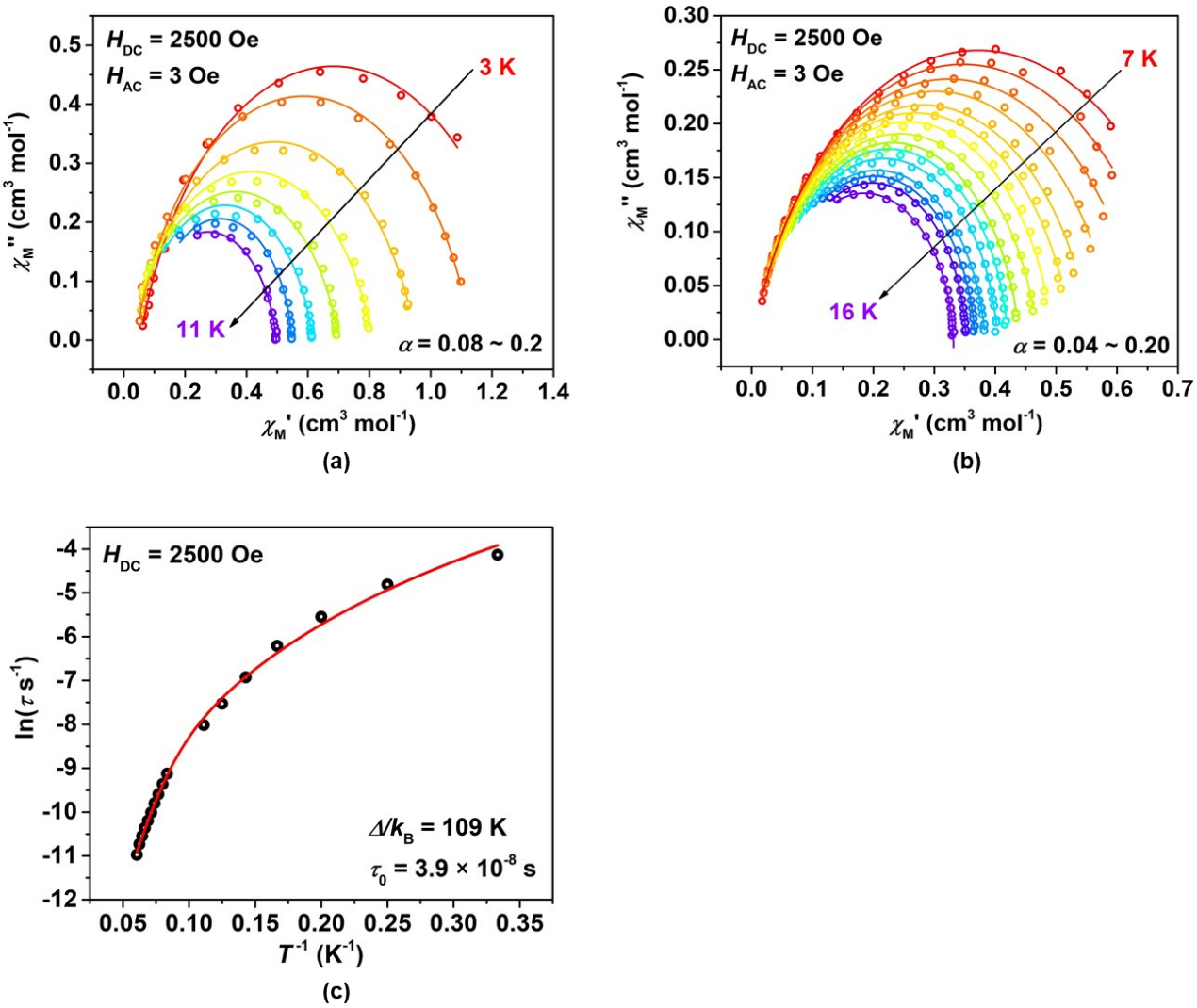

Figure S19. (a) and **(b)**: Argand plots of χ_M'' *vs* χ_M' of **(Dsp)Tm(COT)** under an applied DC magnetic field of 2500 Oe (**(a)** data derived from MPMS, **(b)** data derived from MPMS). **(c)** Plot of natural log of relaxation time versus inverse temperature. The black circles represent the data derived from the measurements. The red solid line represents the best fitting using a combination of Orbach and Raman process. The fitting gives energy barrier Δ/k_B = 109 K and $\tau_0 = 4 \times 10^{-11}$ s.

4. Computational details

Complete-active-space self-consistent field (CASSCF) calculations on the **(Dsp)Tb(COT)**, **(Dsp)Dy(COT)**, **(Dsp)Er(COT)** and **(Dsp)Tm(COT)** (see **Fig. S20** for the complete structure of complex **(Dsp)Tb(COT)**; see **Fig. S22** for the other three complexes) on the basis of X-ray determined geometry have been carried out with MOLCAS 8.2 program package [5], [6].

For CASSCF calculations, the basis sets for all atoms are atomic natural orbitals from the MOLCAS ANO-RCC library: ANO-RCC-VTZP for Tb^{III} (Dy^{III}, Er^{III}, Tm^{III}) ions; VTZ for close C and P; VDZ for distant atoms. The calculations employed the second order Douglas-Kroll-Hess Hamiltonian, where scalar relativistic contractions were taken into account in the basis set and the spin-orbit coupling was handled separately in the restricted active space state interaction (RASSI-SO) procedure. The active electrons in 7 active spaces include all *f* electrons (CAS (8 in 7 for Tb^{III}, 9 in 7 for Dy^{III}, 11 in 7 for Er^{III}, 12 in 7 for Tm^{III}) for complexes **(Dsp)Tb(COT), (Dsp)Dy(COT)**, **(Dsp)Er(COT)** and **(Dsp)Tm(COT)**, respectively) in the CASSCF calculations. To exclude all the doubts, we calculated all the roots in the active space. We have mixed the maximum number of spin-free state which was possible with our hardware (all from 140 quintuplets and 68 from 500 triplets for Tb^{III}; all from 21 sextets, 128 from 224 quadruplets and 130 from 490 doublets for Dy^{III}; all from 35 quadruplets and all from 112 doublets for Er^{III}; all from 21 triplets and all from 68 singlets for Tm^{III}).

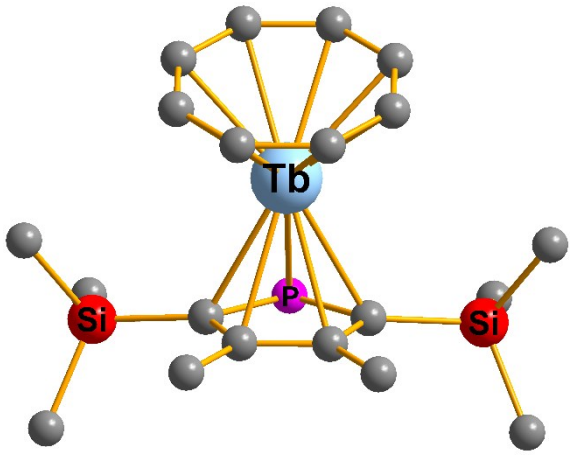

Figure S20. Calculated complete structure of **(Dsp)Tb(COT)**; H atoms are omitted.

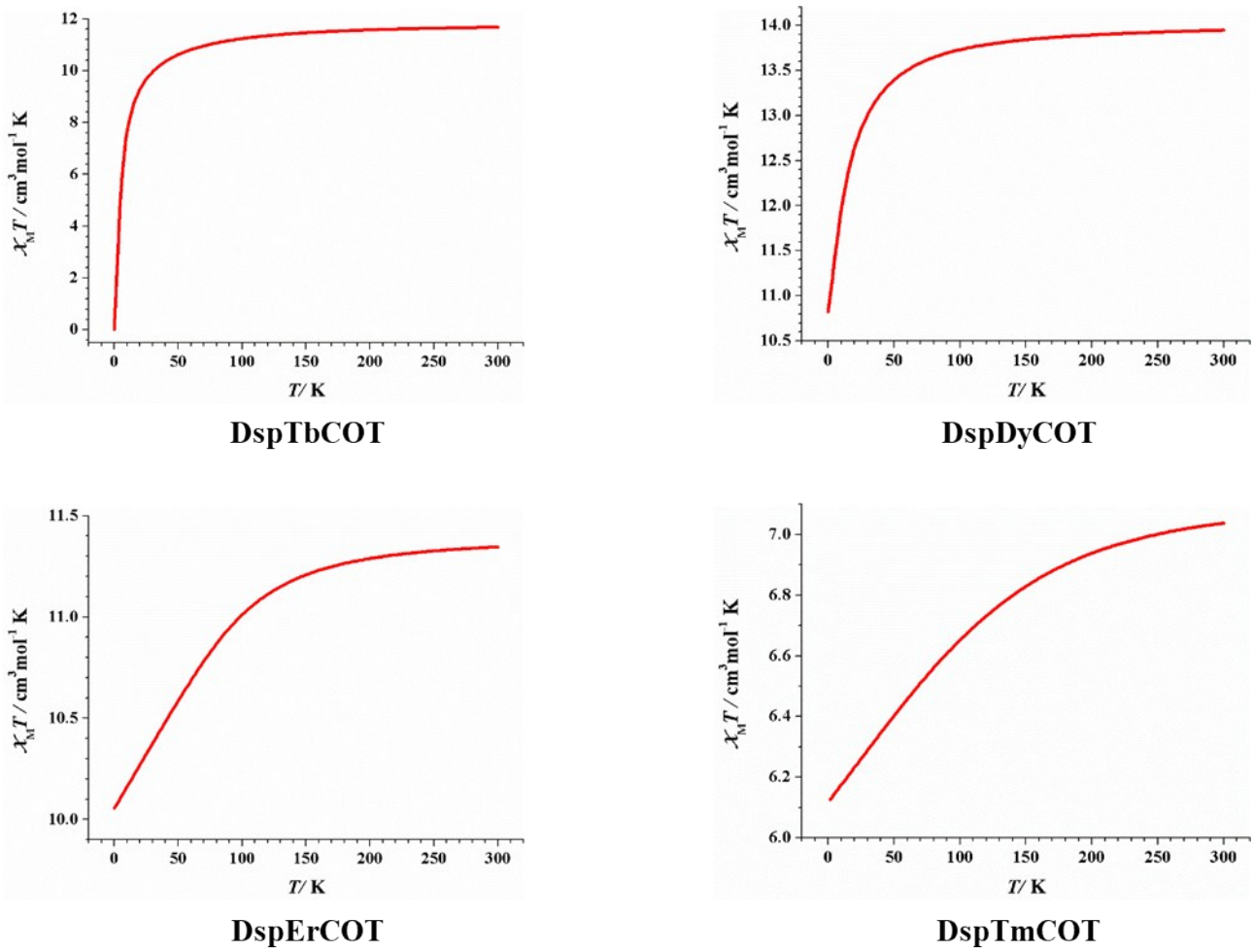

Figure S21. Calculated (solid line) magnetic susceptibility.

Table S4. Calculated energy levels (cm^{-1}), ***g*** (g_x, g_y, g_z) tensors and m_J values of the lowest Kramers doublets of the Dy^{III} (Er^{III}), non– Kramers doublets of the Tb^{III} (Tm^{III}).

	(Dsp)Tb(COT)				(Dsp)Dy(COT)			
	E/cm^{-1}	***g***		m_J	E/cm^{-1}	***g***		m_J
1	0.0	g_x	0.000	±6	0.0	g_x	0.051	±15/2
		g_y	0.000			g_y	0.085	
	11.0	g_z	15.919			g_z	18.608	
2	47.5	g_x		0	33.0	g_x	0.485	±13/2
		g_y				g_y	0.490	
		g_z				g_z	12.601	
3	103.6	g_x	0.000	±2	63.8	g_x	0.513	±3/2
		g_y	0.000			g_y	1.245	
	103.8	g_z	6.183			g_z	7.267	

4	208.3 209.8	g_x g_y g_z	0.000 0.000 9.428	±3	77.3	g_x g_y g_z	0.170 0.200 14.698	±5/2
5	311.3 314.8	g_x g_y g_z	0.000 0.000 15.018	±4	97.1	g_x g_y g_z	9.705 6.660 3.013	±9/2
6	346.3 348.3	g_x g_y g_z	0.000 0.000 15.458	±1	142.0	g_x g_y g_z	0.521 1.840 18.065	±1/2
7	422.6 423.1	g_x g_y g_z	0.000 0.000 16.252	±5	197.9	g_x g_y g_z	0.001 0.003 17.338	±11/2
8					480.6	g_x g_y g_z	0.000 0.000 19.854	±7/2
(Dsp)Er(COT)					**(Dsp)Tm(COT)**			
	E/cm^{-1}	***g***		m_J	E/cm^{-1}	***g***		m_J
1	0.0	g_x g_y g_z	0.0003 0.0004 17.933	±15/2	0.000 0.007	g_x g_y g_z	0.000 0.000 13.989	±6
2	164.3	g_x g_y g_z	0.062 0.081 15.993	±13/2	247.2 247.4	g_x g_y g_z	0.000 0.000 11.745	±5
3	185.1	g_x g_y g_z	0.567 1.956 14.481	±1/2	368.3 373.0	g_x g_y g_z	0.000 0.000 8.979	±4
4	205.3	g_x g_y g_z	7.361 5.627 3.447	±5/2	379.9 381.3	g_x g_y g_z	0.000 0.000 7.777	±2
5	222.6	g_x g_y g_z	0.655 1.303 9.200	±9/2	406.0			0
6	230.3	g_x g_y	0.844 1.434	±7/2	417.2 423.7	g_x g_y	0.000 0.000	±3

		g_z	8.894			g_z	9.022	
7	258.5	g_x	0.348	±3/2	437.7	g_x	0.000	±1
		g_y	0.732			g_y	0.000	
		g_z	14.970		440.2	g_z	0.081	
8	275.4	g_x	0.484	±11/2				
		g_y	0.663					
		g_z	15.454					

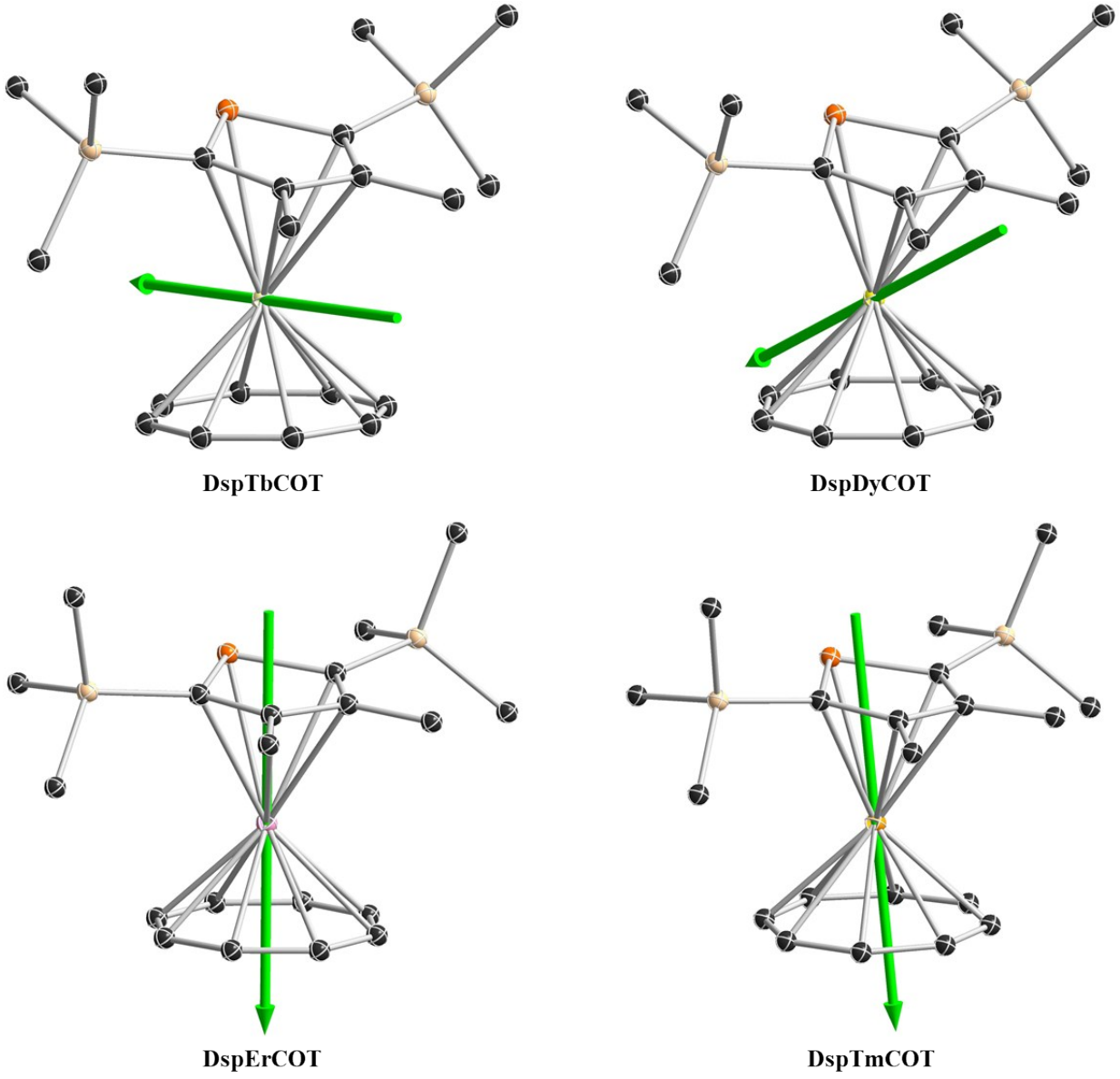

Figure S22. Orientations of the local main magnetic axes (green arrows) of the ground Kramers doublets on Dy^{III} (Er^{III}), non–Kramers doublets on Tb^{III} (Tm^{III}).

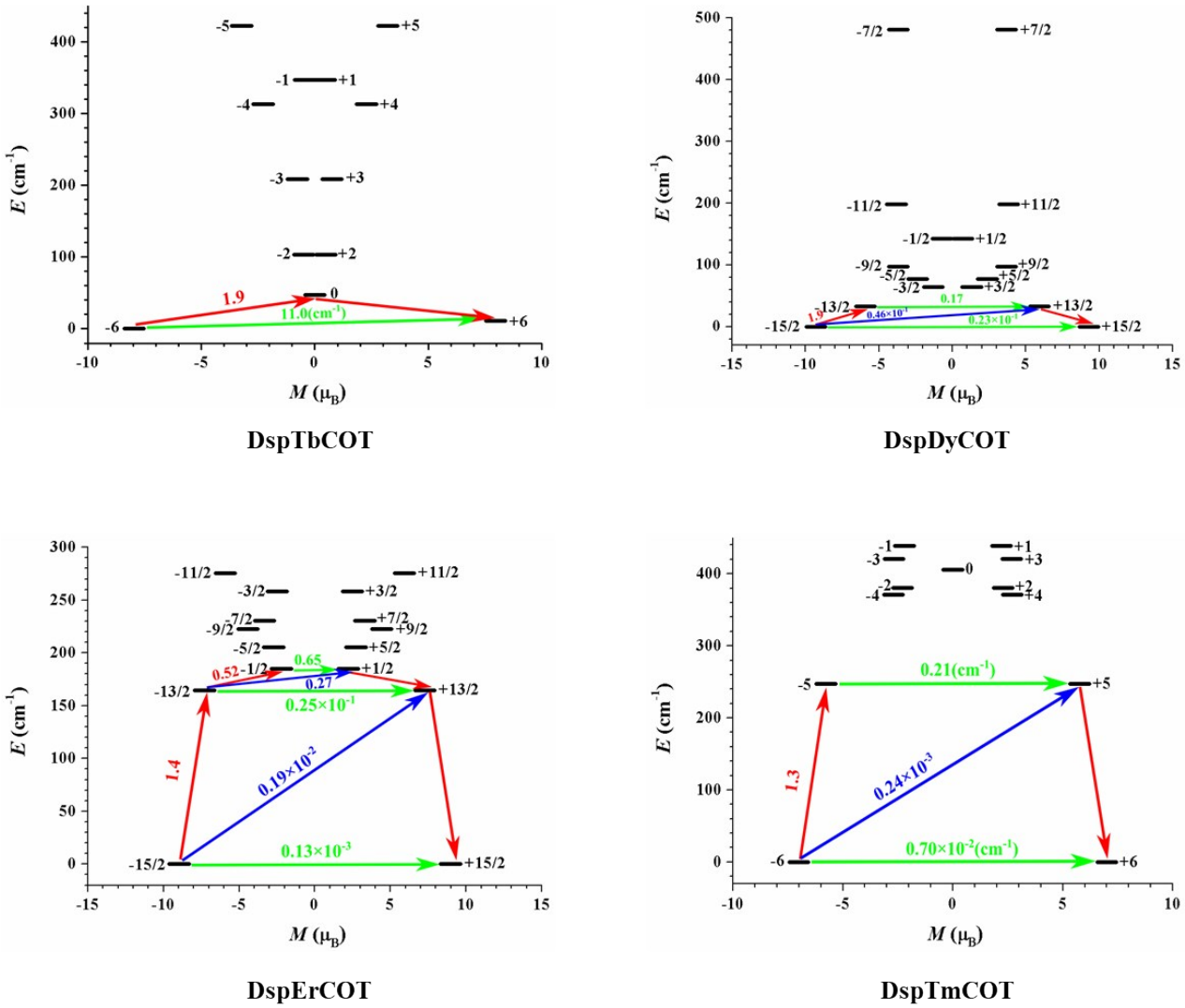

Figure S23. The magnetization blocking barriers in complexes **(Dsp)Ln(COT)**. The thick black lines represent the Kramers doublets for complexes **(Dsp)Dy(COT)** and **(Dsp)Er(COT)**, non–Kramers doublets for complexes **(Dsp)Tb(COT)** and **(Dsp)Tm(COT)** as a function of their magnetic moment along the magnetic axis. The green lines correspond to diagonal quantum tunneling of magnetization (QTM); the blue line represent off-diagonal relaxation process. The numbers at each arrow stand for the mean absolute value of the corresponding matrix element of transition magnetic moment.

In order to build model fragment $[Er(COT)]^+$, COT^{2-} was optimized using *ORCA* 3.0.3 package [7] (RKS, B3LYP/G 6-311G**). The Er^{3+} ion was put on the normal through the center of the COT ring. Series of fragments were obtained by scanning the distance between Er^{3+} ion and the ring center. CASSCF/RASSI-SO/SINGLE_ANISO [8], [9] calculations were performed by using *MOLCAS* 8.1 program [10] to calculate the magnetic properties.

Table S5 Calculated energy levels and g tensors (g_x, g_y, g_z) of the lowest J multiplets for the hypothetical fragment $[Er(COT)]^+$ with series of $d_{Er\text{-}COT}$.

$d_{Er\text{-}COT}$ /Å	1.4				1.5			
	E/cm^{-1}	g_x	g_y	g_z	E/cm^{-1}	g_x	g_y	g_z
1	0	7.475E-06	7.532E-06	17.937463	0	3.163E-06	3.181E-06	17.943501
2	115.716	0.0001609	0.0001663	15.534182	121.024	8.421E-05	8.633E-05	15.538788
3	332.745	0.0001805	0.000204	13.10312	332.009	3.366E-05	0.0001006	13.110411
4	489.096	9.5808476	9.501731	1.2070403	496.686	0.0167299	0.0231416	10.708804
5	502.043	0.030692	0.0323213	10.655429	503.232	9.579738	9.5042279	1.2049406
6	524.563	0.0123466	0.0696392	3.5554663	533.792	0.0111964	0.0606738	3.6085442
7	568.288	3.4444799	3.4488933	5.5049021	569.092	0.589042	4.7985458	9.7204588
8	576.459	3.4279449	3.5044596	7.8315405	573.354	1.5928136	4.8425677	10.79996

$d_{Er\text{-}COT}$ /Å	1.6				1.7			
	E/cm^{-1}	g_x	g_y	g_z	E/cm^{-1}	g_x	g_y	g_z
1	0	1.271E-06	1.284E-06	17.947931	0	5.33E-07	5.84E-07	17.951158
2	128.911	4.54E-05	4.604E-05	15.541522	135.996	2.48E-05	2.494E-05	15.543248
3	327.84	1.686E-05	6.234E-05	13.117585	319.818	3.169E-05	4.495E-05	13.124389
4	481.711	0.0120469	0.012617	10.728131	460.128	0.0077732	0.0079141	10.739985
5	507.885	9.5751588	9.5150923	1.2053371	504.466	9.5724567	9.5204863	1.2036333
6	532.189	0.0053288	0.0548354	3.6523815	522.159	0.0134331	0.0722663	3.9338535
7	553.783	1.0995604	1.8929582	9.7075639	529.133	0.5065181	0.72805	8.7870544
8	561.409	0.5959143	1.930105	10.017821	542.378	0.3200219	0.7823512	9.5702143

$d_{Er\text{-}COT}$ /Å	1.8				1.9			
	E/cm^{-1}	g_x	g_y	g_z	E/cm^{-1}	g_x	g_y	g_z
1	0	0	2.38E-07	17.953498	0	0	2.38E-07	17.955188
2	140.703	1.359E-05	1.36E-05	15.544522	142.754	7.441E-06	7.458E-06	15.545658
3	308.55	3.285E-05	3.498E-05	13.130659	295.253	2.825E-05	2.939E-05	13.13631
4	434.878	0.0050214	0.0050522	10.74984	408.622	0.0032635	0.0032675	10.757679
5	495.113	9.6134074	9.4792207	1.2025563	470.337	0.2085848	0.2136506	8.6939216
6	500.055	0.4104694	0.4278515	9.002735	482.319	9.9734785	9.0736768	1.2131338
7	506.579	0.0145254	0.1006778	3.8911723	487.503	0.407451	0.5046746	4.4559174
8	519.003	0.1222189	0.378947	10.590279	495.192	0.0324672	0.1493866	13.0655

$d_{Er\text{-}COT}$ /Å	2.0				2.1			
	E/cm^{-1}	g_x	g_y	g_z	E/cm^{-1}	g_x	g_y	g_z
1	0	0	2.38E-07	17.956403	0	0	7E-09	17.957271
2	142.583	4.049E-06	4.067E-06	15.546803	141.038	2.243E-06	2.262E-06	15.547986
3	281.305	2.205E-05	2.368E-05	13.141278	268.159	1.755E-05	1.895E-05	13.145451
4	383.546	0.0021224	0.0021366	10.762749	361.498	0.0013985	0.001415	10.764691
5	442.409	0.1244608	0.12552	8.5452508	418.369	0.0769255	0.07739	8.4593034
6	465.616	0.5180031	0.8680538	9.6116673	446.094	0.0312126	0.1494049	6.6770241
7	469.361	8.1083106	8.0295796	1.9844323	456.118	6.5727413	5.5585304	2.1858723
8	475.039	0.1786869	0.5246105	14.015778	460.401	0.8120729	3.8828512	13.801194

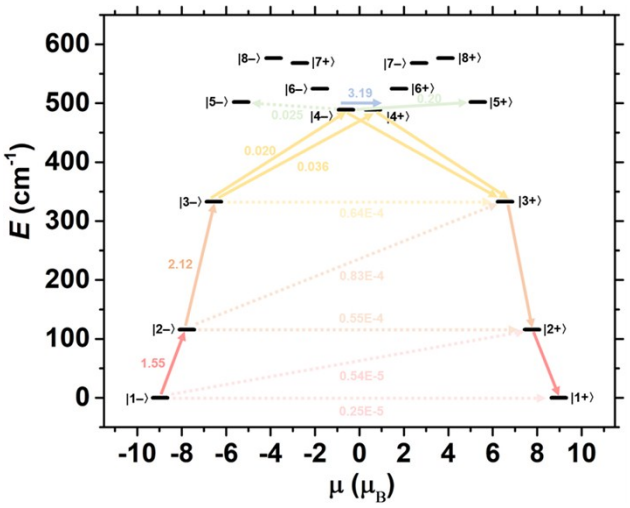

(a) $d_{Er\text{-}COT}$ = 1.4 Å

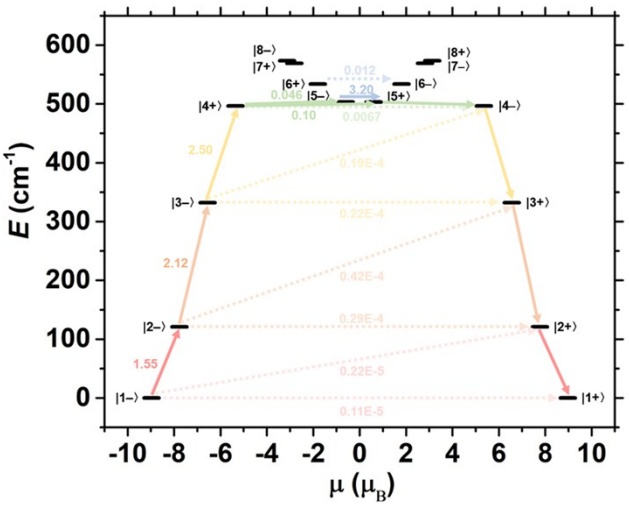

(b) $d_{Er\text{-}COT}$ = 1.5 Å

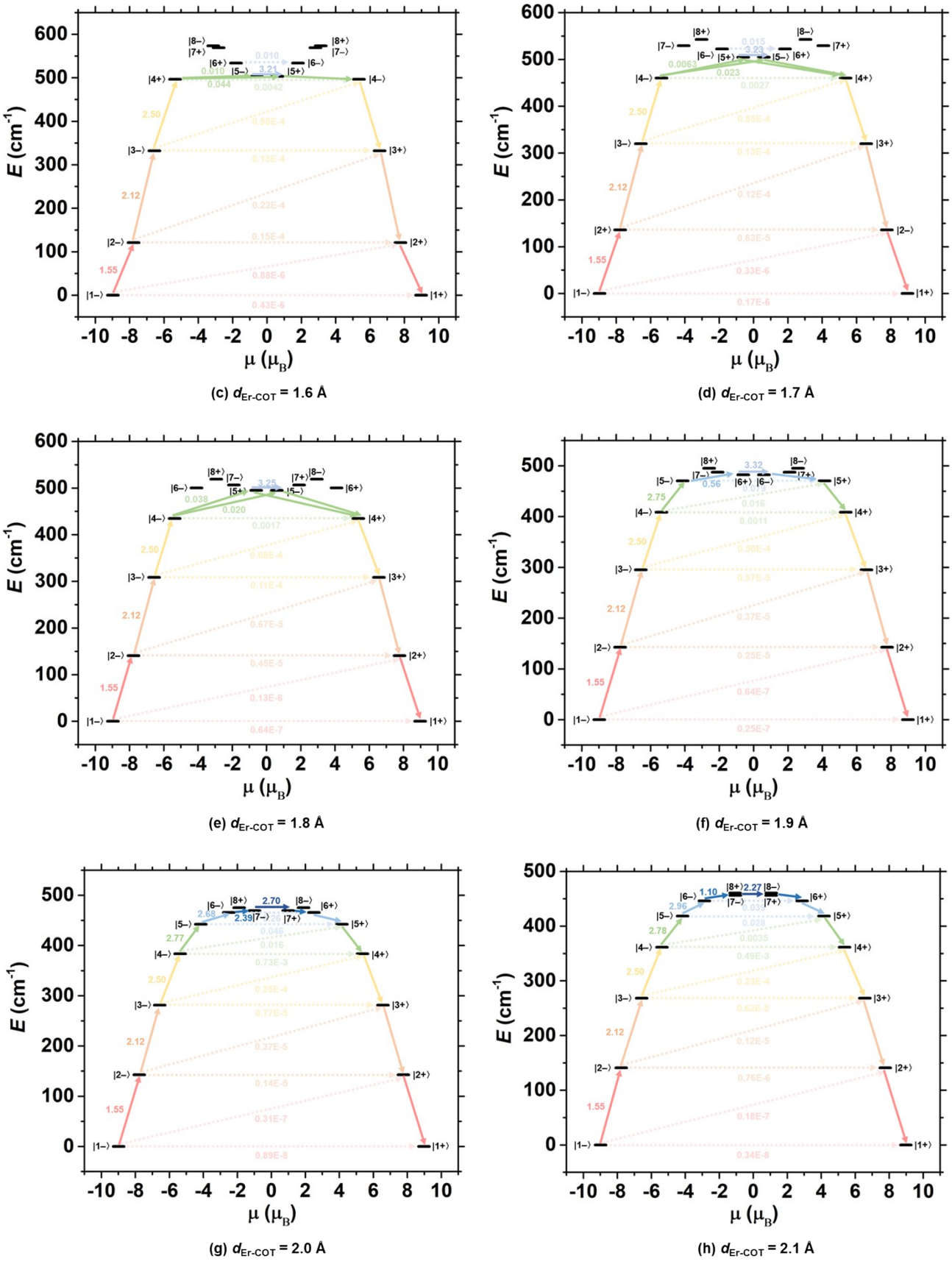

Figure S24. Relaxation of the magnetization for the hypothetical fragment $[Er(COT)]^+$ with series of $d_{Er\text{-}COT}$. The numbers at each arrow stand for the mean absolute value of the corresponding matrix element of transition magnetic moment.

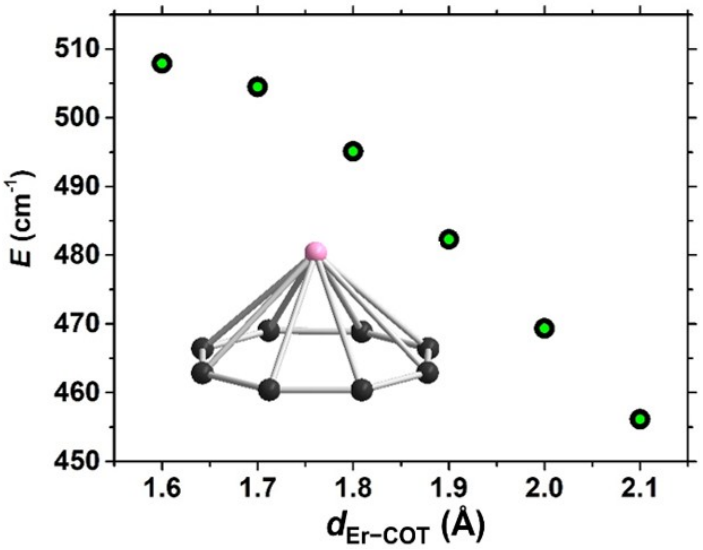

Figure S25. Plot of energy barrier *vs* series of $d_{Er–COT}$ for the hypothetical fragment $[Er(COT)]^+$ calculated based on *ab initio*; inset: $[Er(COT)]^+$.

Table S6 Comparison of $d_{Er–COT}$ and energy barrier for Er-COT series.

Compounds	$d_{Er\text{-}COT}$ (Å)	Error of $d_{Er\text{-}COT}$ (Å)	Energy Barrier (K)
$(C_5H_5BMe)Er(COT)$	1.6743	0.0001	420
$(C_5H_5BH)Er(COT)$	1.6770	0.0003	362
$(C_5H_5BNEt_2)Er(COT)$	1.6796	0.0004	243
(Dsp)Er(COT)	1.6855	0.0003	358
(Cp*)Er(COT)	1.7267	0.0003	273
(Tp)Er(COT)	1.7681	0.0002	179
(Tp*)Er(COT)	1.8177	0.0001	221
$[Er(COT)_2]^-$	1.8747	0.0002	206

Table S7 Comparison of crystal field parameters of (Dsp)Er(COT), (Cp*)Er(COT) and $[Er(COT)_2]^-$.

$$H_{CF} = \sum_{\substack{k=2,4,6 \\ |q|\leq k}} \left(B_k^q \hat{O}_k^q\right)$$

k	q	B_k^q ((Dsp)Er(COT))	B_k^q ((Cp*)Er(COT))	B_k^q ($[Er(COT)_2]^-$)
2	–2	-0.50291783027771E-01	-0.51994077898944E-04	-0.96972625896944E-02
2	–1	0.33774332565701E+00	0.98108667669911E-04	-0.91262441826356E-01
2	0	-0.95417216824644E+00	-0.36425707456849E+00	-0.20860642422908E+01
2	1	-0.43529098314415E+00	-0.18904700557539E+01	0.17775652065138E-01
2	2	0.56512343285453E-01	0.33628707961474E+00	0.18117334234809E+00
4	–4	-0.77737224282435E-04	0.70602958845100E-07	-0.93996936914686E-02
4	–3	-0.37570518929223E-03	0.42296769600490E-05	0.14350810690930E-02
4	–2	0.11559245892501E-02	-0.10312243467669E-06	-0.50134913259304E-04
4	–1	0.49562604411260E-02	0.10147103001287E-05	-0.93911814030286E-03
4	0	-0.46299902193002E-02	-0.44812704617411E-02	-0.57503917542823E-02
4	1	-0.62729385482533E-02	-0.62537833110795E-02	0.37891834458568E-03
4	2	0.42387067475337E-04	0.40531245599767E-03	0.59447164728641E-03
4	3	-0.54284330516269E-03	-0.48635564309710E-02	0.95053049343472E-03
4	4	0.22025621588832E-02	0.13779566826472E-03	0.38498638229010E-01
6	–6	0.11008474118021E-04	-0.38940561322039E-07	-0.96734038811910E-05
6	–5	-0.14704759961568E-03	-0.44779441433267E-06	0.73109148247906E-04
6	–4	-0.50226504591764E-05	0.41116359958015E-08	-0.25356903630612E-03
6	–3	0.13883460169378E-04	0.12502267620404E-06	0.47243550050250E-04
6	–2	0.33890827179461E-04	0.10319032885393E-07	0.82540183652917E-05
6	–1	-0.13898142608431E-03	-0.30945270825841E-07	0.14745894993298E-04
6	0	-0.16641269622589E-04	-0.44750715678113E-04	0.23609897551674E-04
6	1	0.18129837294303E-03	0.36523542088320E-03	-0.33812508205797E-05
6	2	-0.18128675330629E-05	-0.44965627254649E-04	-0.19850828971551E-04
6	3	0.20192895364596E-04	-0.13372235048556E-03	0.35071156161646E-04
6	4	0.58065486136285E-04	-0.21870361655057E-04	0.10382419981987E-02
6	5	0.12960692716446E-03	0.57540393440324E-03	-0.71148479953954E-05
6	6	-0.13314311487222E-04	0.38204992437684E-04	0.18382404833875E-04

5. Copies of ^{1}H NMR and ^{31}P NMR Spectrum of YICOT(THF)$_2$ and DspYCOT

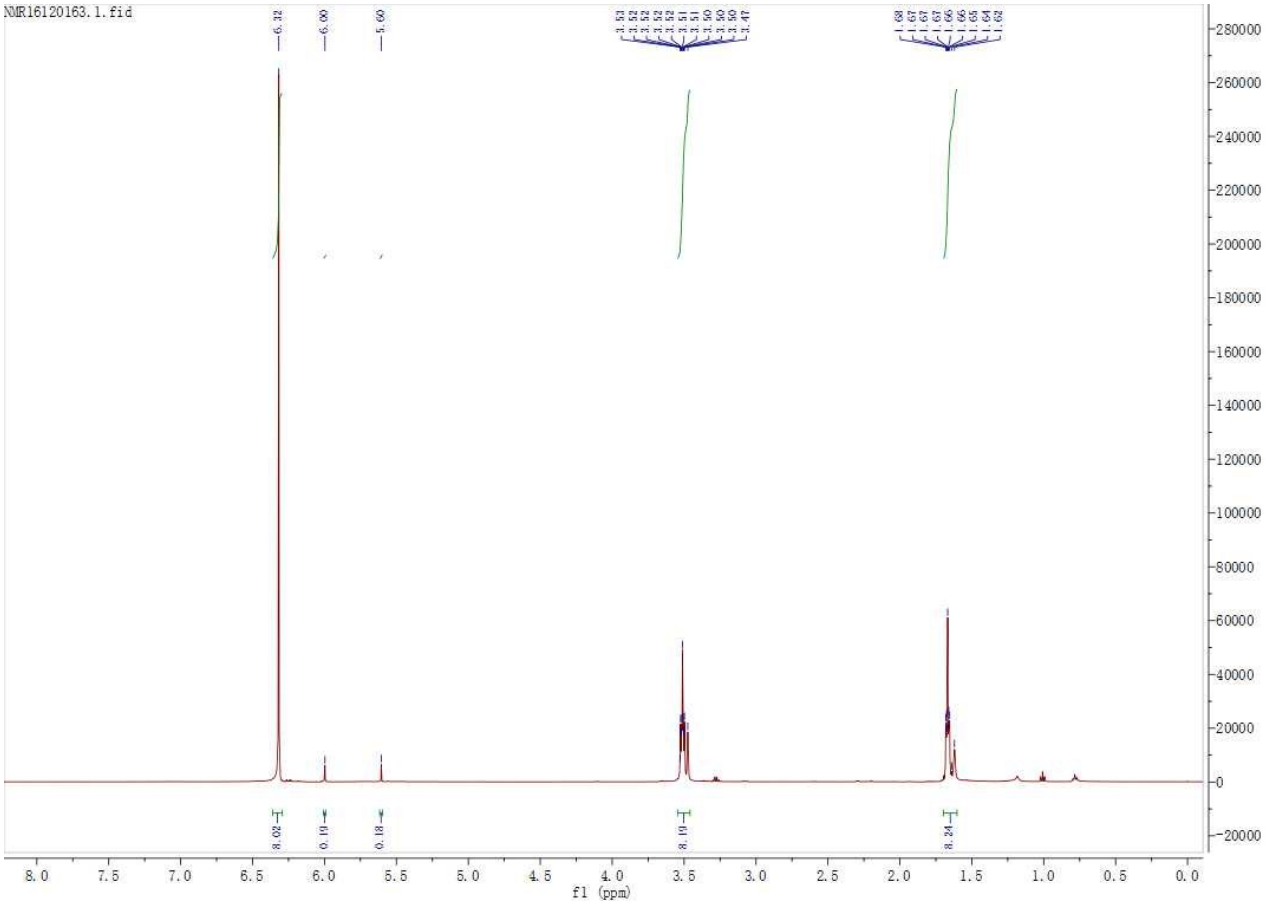

Figure S26. ^{1}H NMR spectrum of YICOT(THF)$_2$.

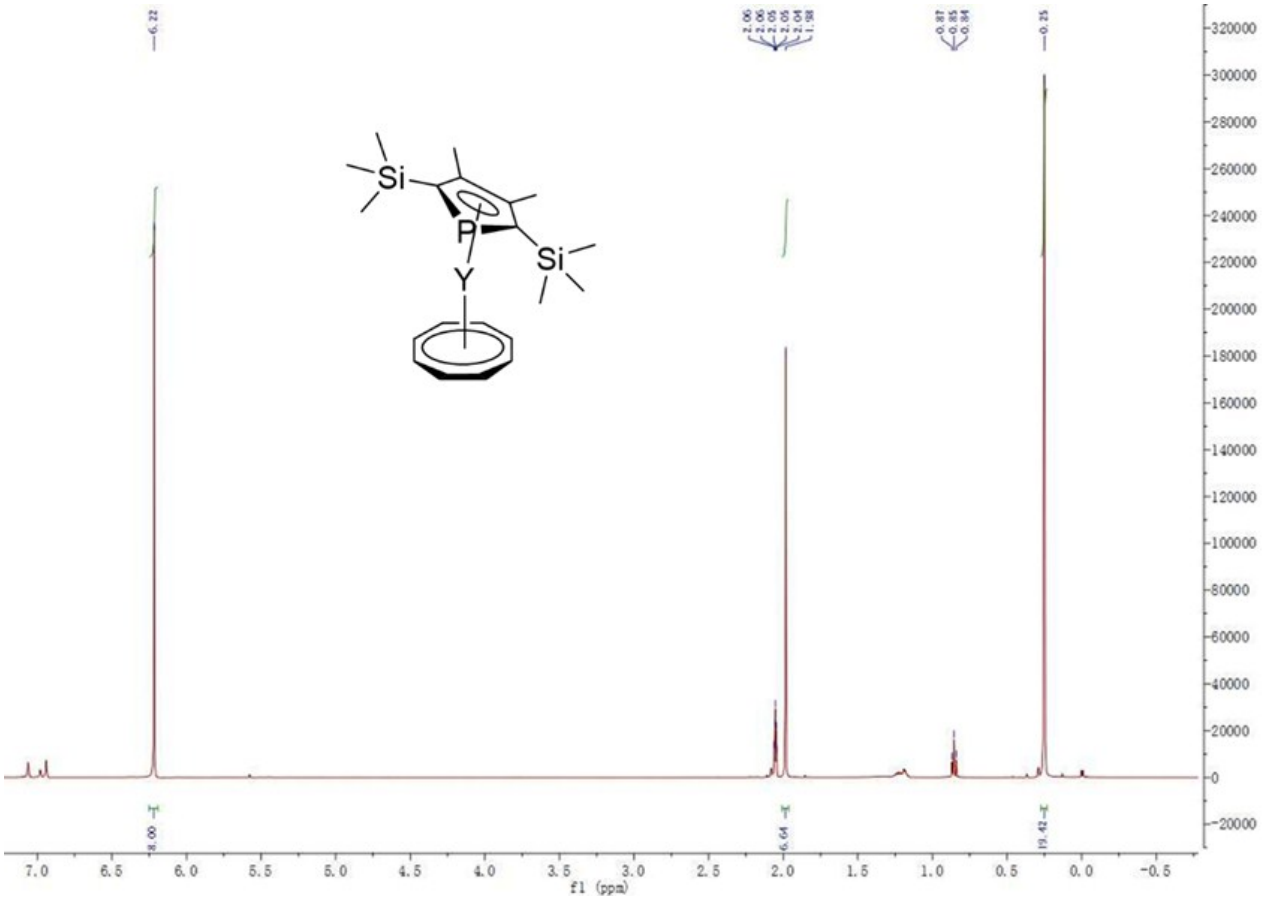

Figure S27. ^{1}H NMR spectrum of DspYCOT.

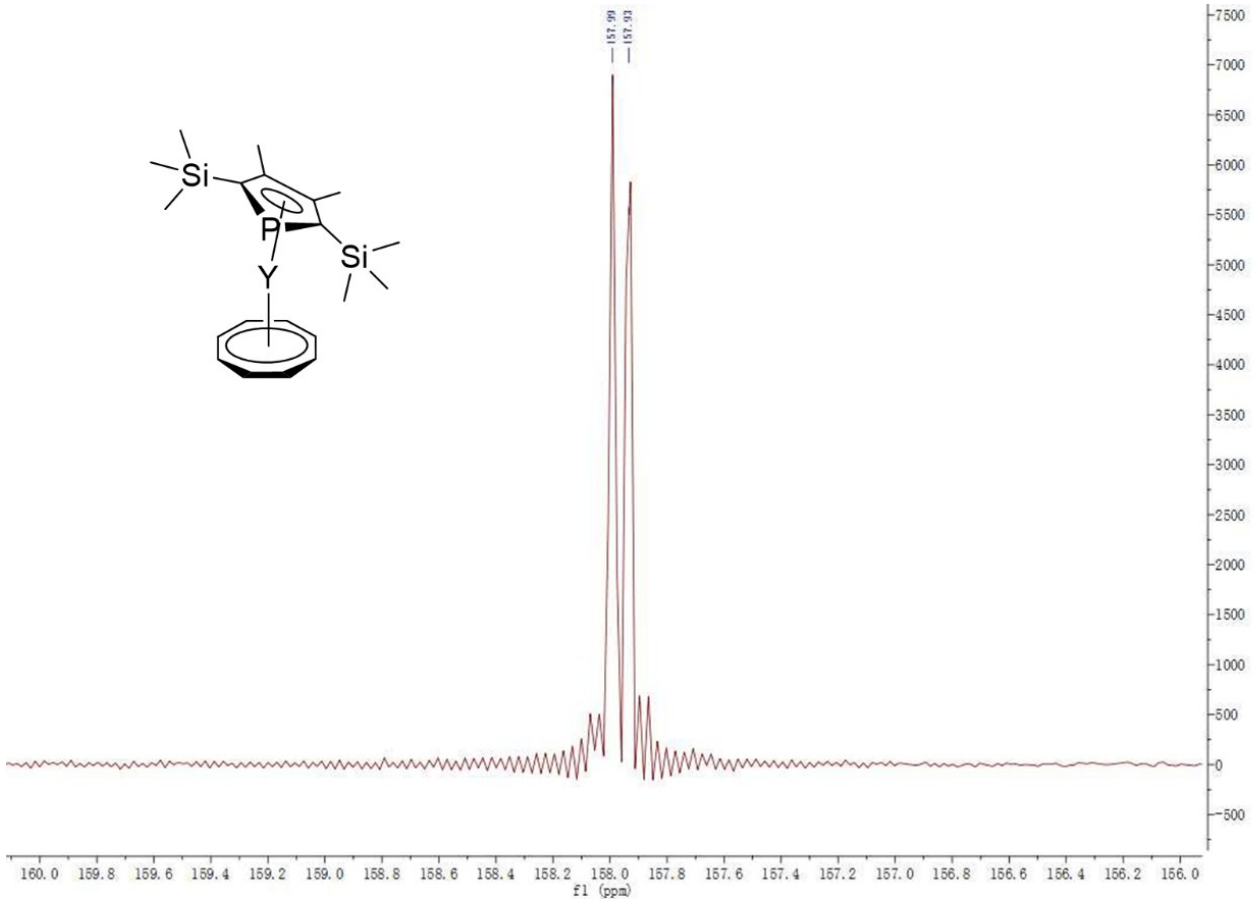

Figure S28. ^{31}P NMR spectrum of DspYCOT.

References

[1] M. Visseaux, F. Nief, L. Ricard. *J. Organomet. Chem.* **2002**, *647*, 139.

[2] A. L. Wayda. *Organometallics* **1983**, *2*, 565.

[3] O. V. Dolomanov, L. J. Bourhis, R. J. Gildea, J. A. K. Howard, H. Puschmann, *J. Appl. Cryst.* **2009**, *42*, 339.

[4] L. Palatinus, G. Chapuis. *J. Appl. Cryst.* **2007**, *40*, 786.

[5] G. A. Bain, J. F. Berry. *J. Chem. Edu.* **2008**, *85*, 532.

[6] G. Karlström, R. Lindh, P. Å. Malmqvist, B. O. Roos, U. Ryde, V. Veryazov, P. O. Widmark, M. Cossi, B. Schimmelpfennig, P. Neogrady, L. Seijo. *Comput. Mater. Sci*. **2003**, *28*, 222.

[7] F. Neese. *Wiley Interdisciplinary Reviews: Computational Molecular Science* **2012**, *2*, 73.

[8] L. F. Chibotaru, L. Ungur. *J. Chem. Phys.* **2012**, *137*, 064112.

[9] L. F. Chibotaru, *et al*., *J. Am. Chem. Soc.* **2008**, *130*, 12445.

[10] F. Aquilante, *et al*., *J. Comput. Chem.* **2016**, *37*, 506.